Metallic and ceramic coatings for enhanced accident tolerant fuel cladding

Chongchong Tang, Michael Stüber, Hans Jürgen Seifert, Martin Steinbrück*

Institute for Applied Materials (IAM-AWP), Karlsruhe Institute of Technology (KIT), D-76021 Karlsruhe, Germany

Email: chongchong.tang@kit.edu, Phone: +49-721/608-28543

Email: michael.stueber@kit.edu, Phone: +49-721/608-23889

Email: hans.seifert@kit.edu, Phone: +49-721/608-23895

Email: martin.steinbrueck@kit.edu, Phone: +49-721/608-22517

Abstract

Zirconium-based alloy fuel claddings applied in current water-cooled nuclear reactors possess multiple desirable attributes during steady-state normal operation. However, the rapid exothermic oxidation reaction between zirconium and steam at elevated temperatures under accident conditions increases system cooling requirements and generates substantial hydrogen, threatening the reactor safety. The Fukushima-Daiichi accidents in 2011 highlighted the demand to develop and implement advanced accident tolerant fuel (ATF) claddings that enhance the safety and reliability of water-cooled nuclear reactors especially during accident scenarios. One near-term evolutionary strategy is surface modification of state-of-the-art zirconium-based alloy cladding with innovative metallic or ceramic coatings. This solution represents an incremental change to the currently standardized UO_2 fuel/Zr alloy cladding structures but allows easier licensing. A variety of coating concepts have been proposed and investigated, including metallic, ceramic or multilayer coatings. This chapter summarizes the research and development status of numerous coating concepts on zirconium alloys for enhanced ATF cladding applications. The principal coating concepts, fabrication methods, performance under normal operations (hydrothermal corrosion/mechanical properties/irradiation behaviors) and under accident scenarios (design-basis/severe) are reviewed and presented.

Keywords

accident tolerant fuel
adherence
ballooning and burst
eutectic reaction
fuel claddings
high temperature
hydrothermal corrosion
irradiation damage
physical vapor deposition
protective coatings
cold spraying
steam oxidation
water-cooled nuclear reactors

Abbreviations

LWRs	Light water reactors
LOCA	Loss of coolant accident
ATF	Accident tolerant fuel
PCMI	Pellet-clad mechanical interaction
HEA	High entropy alloys
PVD	Physical vapor deposition
HVOF	High velocity oxygen fuel spraying
CVD	Chemical vapor deposition
PE-CVD	Plasma-enhanced CVD
DLI-MOCVD	Direct liquid injection of metal organic precursors CVD
BWR	Boiling water reactor
NWC	Normal water chemistry
HWC	Hydrogen water chemistry
SHE	Standard hydrogen electrode
WWER	Water-water energetic reactor
NCD	Nanocrystalline diamond
TMN	Transition metal nitride
DPA	Displacements-per-atom
LTRs	Lead test rods
BDBA	Beyond design basis accident

1 Introduction

Zirconium-based alloys, which were selected and developed as replacements for components made of stainless steel in the 1950s, feature multiple desirable performances, e.g. low thermal neutron absorption cross section, adequate hydrothermal corrosion resistance and good mechanical properties under neutron irradiation, as fuel claddings for light water reactors (LWRs) during steady-state normal operations [1,2]. Advanced nuclear grade zirconium-based alloys, like M5® from Framatome and ZIRLO™ from Westinghouse, exhibiting optimized performances under normal conditions have been deployed via decades of intensive investigation and development and have resulted into exceptionally low failure rates [3]. However, during typical loss of coolant accident (LOCA) or beyond design basis accident (BDBA) scenarios the residual decay heat can lead to rapid core temperature increase and the performance of Zr-alloy fuel claddings are thus highly challenged [4]. One inherent limitation of zirconium-based alloys during accidental scenarios, namely the rapid exothermic zirconium-steam oxidation reaction accompanied by strong heat and hydrogen release, cannot be prevented via optimizing their chemical compositions and/or manufacturing processes [5]. At temperatures beyond 1200°C, the chemical heat release due to the exothermic Zr-steam reaction may exceed the residual decay heat and thus strongly affect the accident progression [4]. The released hydrogen results in the risk of detonation when exposed to oxygen/air. **(see Chapter x.xx Steam Oxidation in Accident Scenarios)** In addition, zirconium alloy claddings can absorb significant amounts of hydrogen during both normal and accident conditions. Hydrogen can dissolve or precipitate as brittle hydrides in the matrix. **(see Chapter x.xx Zirconium Alloys: Properties and Characteristics).** Hydrogen embrittlement dramatically degrades the mechanical performance of zirconium alloy claddings, limiting fuel burnup under normal operations and challenging the physical integrity of the cladding tube especially during accident conditions [6].

The Fukushima Daiichi Accidents in 2011 highlighted the detrimental performance characteristics of the zirconium-based alloy fuel claddings during (severe) accidental scenarios and the need to develop advanced accident tolerant fuel (ATF) claddings for enhancing the safety margins of water-cooled reactors [7]. Advanced ATF materials should tolerate the loss of active cooling inside the core for a considerably longer period of time and up to higher temperatures (>1200°C) relative to the standard UO_2/Zr-alloy clad fuel system offering additional coping time for severe accident management. In the meantime, they must demonstrate the potential for maintaining or improving fuel performance during normal operating conditions [8]. A variety of ATF cladding concepts have been proposed and evaluated worldwide [7–11]. One approach is to replace the state-of-the-art Zr-based alloy cladding with new materials exhibiting much lower steam oxidation kinetics resulting in less heat and hydrogen production. This approach comprises mainly three types of materials, namely FeCrAl-based alloys [12], lined Mo-alloy cladding [13] and SiC_f/SiC composites [14]. These potential accident-tolerant cladding alternatives using novel materials remain a long-term solution that may require substantial redesign of the reactor core. Another more near-term evolutionary strategy can be

surface modification of the zirconium-based alloy cladding with an innovative high-temperature oxidation/corrosion resistant metallic or ceramic coating [10]. This solution, assuming thin coatings, represents an incremental change to the current UO_2 fuel/Zr-alloy clad structures and allows easier licensing.

Decorative and functional coatings have seen numerous applications in a wide range of engineering systems; some recognizable examples include photochromic coatings, hard nitride coatings and thermal barrier coatings, etc. A variety of processes are also commercially available to fabricate the coatings [15]. Depending on the coating applications, one or often multiple primary functional properties are required. The extremely harsh environments inside the nuclear core obviously demand robust coatings that can fulfill stringent performance requirements and technical specifications [16]. An ideal ATF coating or coated Zr-alloy cladding is foreseen to meet the following unique requirements [10,11]:

- reduced hydrothermal corrosion rate and stored hydrogen inventory during normal operations;
- high adherence and ductility to sustain a high level of deformation and stress (for instance, irradiation induced swelling and creep, pellet-clad mechanical interaction [PCMI], clad ballooning);
- chemical and mechanical compatibility with the Zr-alloy cladding substrate during normal and off-normal conditions;
- significantly reduced oxidation kinetics in high-temperature steam/air atmosphere and higher mechanical strength leading to increased coping time relative to bare Zr-alloy cladding during accident scenarios;
- adequate coating thickness to provide enhanced accident tolerance as well as negligible impact on fuel performances (including neutron economy, fuel temperature, critical heat flux, etc.) within the core;
- capability to coat full-length cladding tube at low temperature (<500°C) with excellent process stability and reproducibility.

The two basic yet prerequisite requirements of materials considered as coatings for enhanced ATF cladding applications are their resistance to hydrothermal corrosion (normal operations) and to high-temperature steam/air oxidation (accidental scenarios). Both working environments demand the growth of a thermodynamically stable, adherent oxide layer on the surface that acts as an effective diffusion barrier [7]. Development and validation of various proposed coating concepts to date mainly focus on determining their protective capability under one or both regimes simulating out-of-pile conditions. This chapter reviews current research and development status of numerous metallic and ceramic coating concepts on Zr alloys for enhanced ATF cladding.

2 Principal coating concepts

The majority of studies on surface modification of Zr-based alloys was initiated after the Fukushima accidents; the few studies prior to Fukushima focused on improving their hydrothermal corrosion resistance to withstand higher burnup [17,18] and alleviating vulnerability to grid-to-rod fretting failure [19]. A wide variety of materials have been proposed and examined as protective coatings on Zr alloys. The principal coating concepts can be broadly divided into three categories: metallic coatings, ceramic coatings and multilayer coatings, as summarized in Table 1. Some less relevant coating concepts or surface modification methods are not considered here [10]. Nearly all coating concepts consider only protection of waterside (outer) surfaces of the cladding tube. In case of accidental scenarios such as LOCA with ballooning and burst of the cladding, oxidation of fuel side (inner) surfaces may become significant as well. To our knowledge, only one group focused on enhanced protection of the inner surface based on amorphous Cr-based coatings deposited by DLI-MOCVD (Direct Liquid Injection of Metal Organic precursors Chemical Vapor Deposition) process [20,21].

Table 1 *Summary of different types of proposed coating materials on Zr alloys as coated ATF claddings*

Metallic coatings	Single element	Al, Si, Cr
	Intermetallic/Alloy	Zr-Si, Cr-Al, CrAlSi, FeCrAl, AlCrMoNbZr (HEA)
Ceramic coatings	Oxide	Al_2O_3, Cr_2O_3, ZrO_2
	Carbide	C (CVD diamond), SiC, CrC, ZrAlC
	Nitride	TiN, CrN, TiAlN, CrAlN, CrAl(Si/Ti)N
	MAX Phase	Ti_2AlC, Cr_2AlC, V_2AlC
Multilayer coatings	Ti/TiN, Cr/CrN, Al/Al_2O_3, Cr/CrAl, Mo/FeCrAl, ZrO_2/FeCrAl, TiC/Ti_2AlC, $ZrSi_2$/Zr_2Si, TiN/TiAlN, AlCrMoNbZr/(AlCrMoNbZr)N	

**Note that Si and C (CVD diamond) are classified as metallic and carbide here for simplicity.*

Coating materials with low density, high melting point and thermal conductivity, comparable thermal expansion coefficient to Zr alloy substrate and low neutron absorption cross section are favorable [22]. Table 2 gives the values of some notable properties of these coating materials, together with Zircaloy-4 as comparison (mainly adopted from MatWeb database). Both single metallic element and intermetallic/alloy have been examined. A pure metallic chromium coating represents an attractive and encouraging choice as a near-term ATF solution for implementation considering its satisfactory compromise of performance under both normal and accident conditions. Thus, Cr coatings are being intensively pursued by both academia and industry [2324252627282930313233], [3435363738394041424344], [45464748495051525354555 6]. Among the metallic materials, one new alloy concept denoted as high entropy alloys (HEA) (or multi-principal component alloys) was explored recently [57]. HEAs are loosely defined as solid solution alloys that comprise at least

five principal elements in equal or near equal atomic concentration [58]. The specific random arrangement of atoms in HEAs endows them some exceptional physical and mechanical properties [58]. Metallic coating materials typically offer the benefits of excellent adherence, high toughness and ductility, high thermal conductivity and easy fabrication. However, they normally possess low melting temperature or low eutectic reaction temperature with underlying Zr alloy substrate, challenging their performances during accident scenarios.

Ceramic coatings investigated include oxides, carbides, nitrides and one family of ternary-layered compound $M_{n+1}AX_n$ (MAX, n typical 1-3) phases. The MAX phase (M: early transition metal, A: mainly A-group element and X: C and/or N) materials are layered, hexagonal carbides and nitrides [59,60]. Their crystal structures can be viewed as different transition metal carbide or nitride layers interleaved by pure A-element layer. They have attracted increasing attention in recent decades because of their unique combination of metallic and ceramic properties. Ceramics generally exhibit excellent corrosion resistance and radiation tolerance, high hardness and good wear resistance [10,61]. One critical challenge to be evaluated for ceramic materials as protective coating is their brittle characteristics and low fracture toughness, making them susceptible to cracking/spallation when suffering high stresses.

To overcome or alleviate the limitations of a single-layer metallic or ceramic coating, many multilayer coating designs have been proposed, as shown in Table 1. For instance, a thin metallic layer as a bonding interlayer aims to improve the adhesive strength of ceramic coatings [62,63]; diffusion barriers were designed to alleviate the eutectic reaction or rapid interdiffusion between the coating and the Zr alloy substrate during high-temperature oxidation [28,64]. Since silica and alumina are unstable and undergo hydrothermal dissolution as silicic acid (H_4SiO_4) and aluminum oxy-hydroxide (AlO(OH)), respectively, during normal operation conditions (see section 4.1), functional layered coatings consisting of both corrosion- and oxidation-resistant layers simultaneously in a multilayer sequence were proposed [65,66]. In addition, multilayer coatings often provide enhanced mechanical properties and corrosion performance compared to single layer coatings; the repetitive re-nucleation mechanism of defects at each interface enable interfaces to act as barriers to restrain the expansion and propagation of undesirable defects, such as micro-cracks and pores, within the coatings [67,68]. However, the interfaces could diminish heat transfer in the coatings; for example, reduced thermal conductivity with increasing sublayers (interfaces) have been observed in TiN/TiAlN multilayer coatings [69]. Moreover, the multilayer designs add complexity in fabrication procedure and quality control of the coatings.

Table 2 Summary of selected physiochemical properties of principal coating materials

	Density (g/cm^3)	**Melting/Solidus temperature (°C)**	**Thermal expansion coefficient ($\times 10^{-6}$ K^{-1}, RT)**	**Thermal conductivity (W/(m·K), RT)**
Zircaloy-4	6.56	1850	6.0	21.5
Al	2.70	660	23.2	237
Si	2.33	1410	2.6	148
Cr	7.14	1850	6.7	93.7
Mo (barrier)	10.28	2623	4.8	138
$ZrSi_2$	4.88	1620	~30	-
FeCrAl (Kanthal APM)	7.10	1500	11.0	11
HEA (AlCoCrFeNi)	~6.50	~1300	12-16.5	10-22
Al_2O_3	3.96	2044	8.1	~18
Cr_2O_3	5.22	2330	7.1	~12
ZrO_2	5.68	2715	7.0 (monoclinic) 12.0 (tetragonal)	1.67 (monoclinic)
CVD diamond	2.26	3650 (sublimation)	~1.0	> 120
3C-SiC	3.10	2830 (decomposition)	~4.4	> 140
Cr_7C_3	6.5-7.0	~ 1765	-	-
TiN (TiAlN) coating	5.22	2930	7-10	5-12
CrN (CrAlN) coating	5.90	1770	~9.0	2-5
Ti_2AlC	4.00	> 3000 (decomposition)	~8.5	46
Cr_2AlC	5.24	~ 1500 (decomposition)	~12.5	22
V_2AlC	4.87	-	~9.4	45

**RT represents room temperature.*

3 Deposition/Fabrication methods

Several fabrication technologies have been used to deposit coatings on Zr alloys; the nature and performance of coatings depend significantly on the adopted fabrication technology and concurrent processing parameters. Physical vapor deposition (PVD, including magnetron sputtering, cathodic arc evaporation, electron beam evaporation, pulsed laser deposition, ion plating) and spraying (like cold spraying, plasma spraying and high velocity oxygen fuel (HVOF) spraying) represent the two most popular application methods for ATF claddings [10].

In the PVD process, coating materials are vaporized from a solid or liquid source by heat or by bombardment with energetic particles in a vacuum or low-pressure gaseous (plasma) environment and finally condense onto the substrate [70]. Most PVD methods can coat the substrate at low temperatures (typically below 500°C) with dense, smooth and relatively thin layers (5-30 μm). The low deposition temperature and thin coating thickness are preferred with respect to the negligible impact on the microstructure of the cladding substrate and on the neutronic penalties inside the core, respectively [66,71,72].

In spraying processes, material particles or droplets are accelerated to high velocities and impinge on the surface of the substrate to form a coating via kinetic energy transfer. Depending on the processing temperature of the feedstock powder, cold spraying and thermal spraying processes exist. Most sprayed coatings for the ATF application adopted cold spraying because of its low process temperature and minimal oxidation. Spraying methods normally fabricate thick coatings (>30 μm) with a high deposition rate, but with the drawbacks of less uniform and less dense layers. **Figure 1** displays typical microstructures of one metallic coating (Cr) and one ceramic coating (Ti_2AlC) on Zr alloys deposited by PVD and cold spraying. The noticeable differences in the microstructure of same type of coatings deposited via distinct methods can be seen. An uneven surface and coating/substrate interface (presence of Kelvin-Helmholtz perturbations) [73,74] and some porosity exist for the cold spraying coatings. To fulfill the required surface quality, a post-polishing process has been developed to smooth cold-sprayed Cr [32,54] or FeCrAl [64] coatings. In addition, the mechanical impact of the high-velocity particles in the cold spraying process may result in a high level of residual stresses and severe plastic deformation of the bulk surface [73], altering the mechanical characteristics of the substrate (see section 4.2).

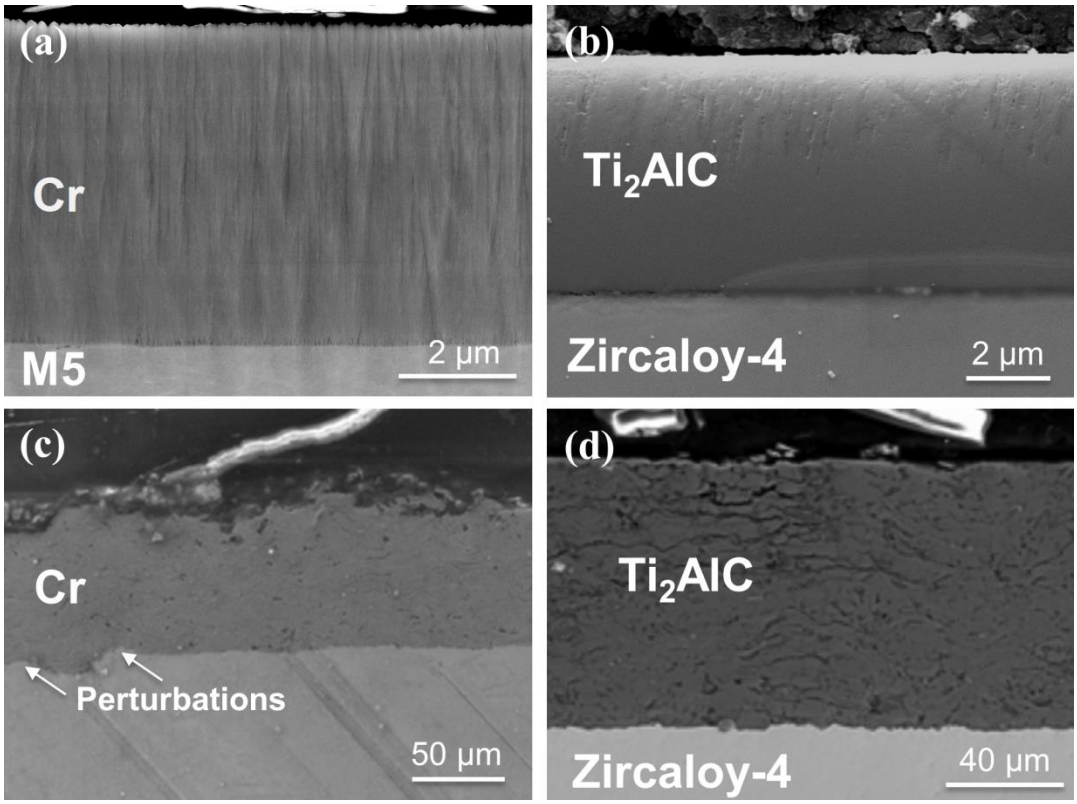

Figure 1 *Typical microstructures of metallic (Cr) and ceramic (Ti_2AlC) coatings on Zr alloys deposited by different processes: (a) and (b) PVD process; (c) and (d) cold spraying process.* [49,53]

Chemical vapor deposition (CVD) and laser cladding technology have also been used for deposition of coatings on Zr alloys. The CVD process involves decomposition and/or reaction of volatile precursors to yield the desired films on the surface of substrates via chemical reaction at relatively high temperatures [15]. For instance, Kaushal et al. attempted to deposit SiC coatings on Zr alloy substrate using a synthesized organosilicon precursor at 900°C [75]. Certain proprietary low temperature plasma-enhanced CVD (PE-CVD) techniques have been developed; for example, synthesis of a SiC coating at approximately 370°C [76] and polycrystalline diamond film at approximately 600°C [77]. Michau et al. successfully coated the inner surface of cladding tube with Cr-based coatings (Cr, CrC or CrSiC) by DLI-MOCVD at around 500°C [21]. Typically, reducing the deposition temperature in CVD will simultaneously diminish the deposition rate [78]. Thus, the efficiency and homogeneity of the coatings deposited by these low-temperature CVD processes need further assessment. Laser cladding technology uses a powerful laser beam to melt the injected powder to form, after solidification, a coating layer. Cr, CrAl and Ni–Zr intermetallic/ceramic reinforced composite coatings have been fabricated on Zr alloys by this technology [26,79,80]. This method offers the benefits of high deposition rate with highly dense and adherent coatings, but less uniformity. The effects on structural performances of the substrate due to heating effect have to be established.

Some other methods, including electroplating [81], plasma electrolytic oxidation [82] and pre-oxidation [83], are occasionally used. Additionally, surface modification using

laser beam scanning to produce an oxide dispersion strengthened (ODS) structure on the Zr alloy surface before coating deposition for improving the high temperature strength was investigated [84,85]. These methods, however, appear to be less attractive for practical applications due to some undesirable features (for instance coatings that are too thick or too rough, high processing temperatures, etc.).

To achieve optimized performance, the coating processes are normally subjected to an optimization procedure. For technical application, adjusting the process parameters to improve deposition efficiency and to optimize coating performances are regularly carried out [37,53,55,62,86]. Deposition of phase-pure MAX phase coatings often remains a challenging issue due to their highly ordered crystal lattice structures and potential growth of many competitive compounds [60]. Recently, Tang et al. demonstrated that textured and single Cr_2AlC and Ti_2AlC MAX phase coatings can be synthesized on Zr-alloy substrates via controlled thermal annealing of magnetron-sputtered nanoscale elemental multilayers [87]. However, the successful transfer of this laboratory-scale process to industrial application level needs to be proved. The feasibility of fabricating full-length Cr-coated cladding tubes via PVD was recently demonstrated [45].

4 Performance under normal operation conditions

While enhancing the accident tolerance of fuel claddings is desired, one prerequisite is that the coatings should withstand the harsh environments inside the reactor core during normal operation.

4.1 Hydrothermal corrosion behavior

Pressurized water is used as the coolant in light water reactors. Depending on the type of the reactor, three distinct water chemistry environments exist, i.e. PWR (pressurized water reactor, ~330°C, 15.5 MPa), BWR (boiling water reactor, ~285°C, 7.5 MPa)-NWC (normal water chemistry) and BWR-HWC (hydrogen water chemistry). The water chemistry is optimized via minor additives to ensure reliable performance of reactor components. **(see Chapters x.xx Corrosion of Zirconium Alloys and x.xx Water chemistry)**

The combination of high temperature and pressure results in coolant water in a subcritical state that acts as a highly corrosive medium. Thus, the waterside surfaces of the fuel claddings are exposed to hydrothermal corrosion. Many metallic or non-oxide ceramic materials are converted into their oxides or dissolve rapidly during hydrothermal corrosion in hot water [88]. Materials (exclusive of oxides) enable good hydrothermal corrosion resistances that can grow a passivation oxide layer acting as an effective diffusion barrier. The nature of a material, mostly metals, undergoing electrochemical corrosion in aqueous solutions can be predicted by Pourbaix diagrams, i.e. electrochemical potential versus pH diagrams for a given

temperature, pressure and dissolved ion concentration via thermodynamic calculations [89]. **Figure 2** displays the Pourbaix diagrams of Si, Al, Ti and Cr at 350°C, 25 MPa and 10^{-6} mol/kg (typical operating conditions for PWR with slightly higher pressure), as examples. The diagrams can be classified into three regimes of immunity, passivity, and corrosion according to the identities of the dominant species: unreacted metal, stable surface oxide, and aqueous ions, respectively. Obviously, under typical PWR normal conditions as shown in **Figure 2**, SiO_2 and Al_2O_3 are non-stable via formation of soluble aqueous ions. Rapid hydrothermal dissolution or selective leaching of these two elements (or oxides) may happen for Si- and Al-containing coatings. Metallic Ti and Cr (plus Zr, Fe and Ni [10,89–91]) or compounds of corresponding metal-based coating materials are expected to form a stable, passive oxide layer. As summarized below, the corrosion performance of coating materials examined under simulated PWR normal conditions are largely consistent with the chemical nature predicted by Pourbaix diagrams.

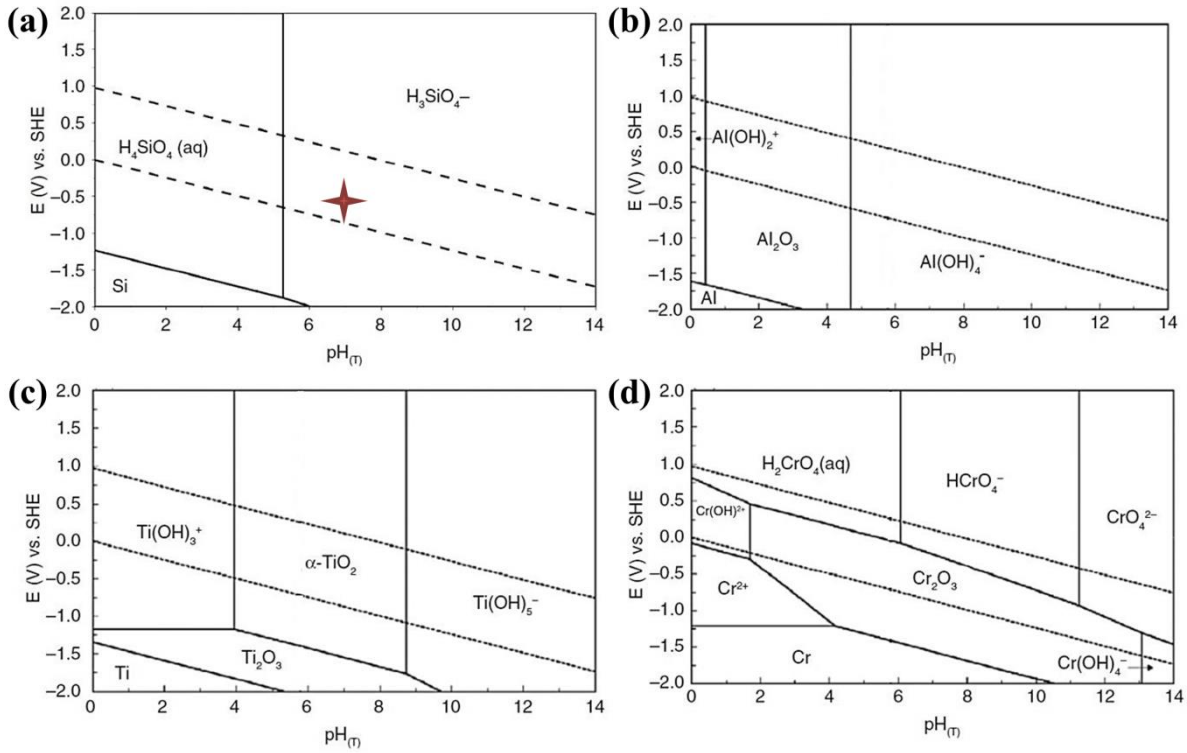

Figure 2 *Pourbaix diagrams for (A) Si, (B) Al, (C) Ti and (D) Cr at 350°C, 25 MPa and 10^{-6} mol/kg. [10] SHE indicates standard hydrogen electrode. The electrochemical potential and pH for the aqueous solution in PWR core are approximately −0.5 V_{SHE} and 7.0, respectively, marked as star symbol in (A).*

4.1.1 Metallic coatings

Al and Si: To date, the hydrothermal corrosion behavior of pure Al and Si coatings on Zr alloys has not been reported. However, Park reported that amorphous alumina coatings were not stable and converted to γ-AlO(OH) (Boehmite) during autoclave exposure at 20.1 MPa and 343°C [92]. The hypothesized mechanisms were the dissolution of amorphous alumina and subsequent re-precipitation of boehmite during the cooling process. Kim et al. have tested bulk Si wafer and SiO_2 samples in a pressured water condition at 18.9 MPa and 360°C; rapid dissolution was confirmed for both samples [26]. Thus, pure Al and Si (as well Al_2O_3 and SiO_2) coatings, as expected, cannot survive under normal operating conditions.

Cr: Formation of a superficial, thermodynamically stable Cr_2O_3 layer bestows the Cr-coated claddings with an extremely low corrosion rate under simulated normal operational conditions, as experimentally proven by several groups [26,41,48,53]. **Figure 3** compares the mass gain and oxide scale thickness between uncoated and PVD Cr-coated Zr alloys during hydrothermal corrosion in an autoclave. A considerably lower mass gain of the Cr-coated claddings compared to the uncoated ones was confirmed under both PWR water chemistry and WWER (Russian PWR) water environments during long-term exposure. The thickness of the oxide scale formed on a Cr coating is roughly one order of magnitude thinner than the ZrO_2 layer growth on an uncoated alloy after exposure at 360°C and 18.7 MPa for 60 days, as shown in **Figure 3** (b) and (c). Similar results were obtained during autoclave tests of PVD Cr coatings at 415°C and 10 MPa, cold spraying and laser cladding Cr coatings under PWR conditions. The Cr_2O_3 layer can also act as a more efficient hydrogen diffusion barrier, lowering the hydrogen pickup of the cladding matrix during normal operation [48]. Therefore, Cr-coated claddings will be more tolerant to hydrogen embrittlement and allow for increased operational margins and higher fuel burnup.

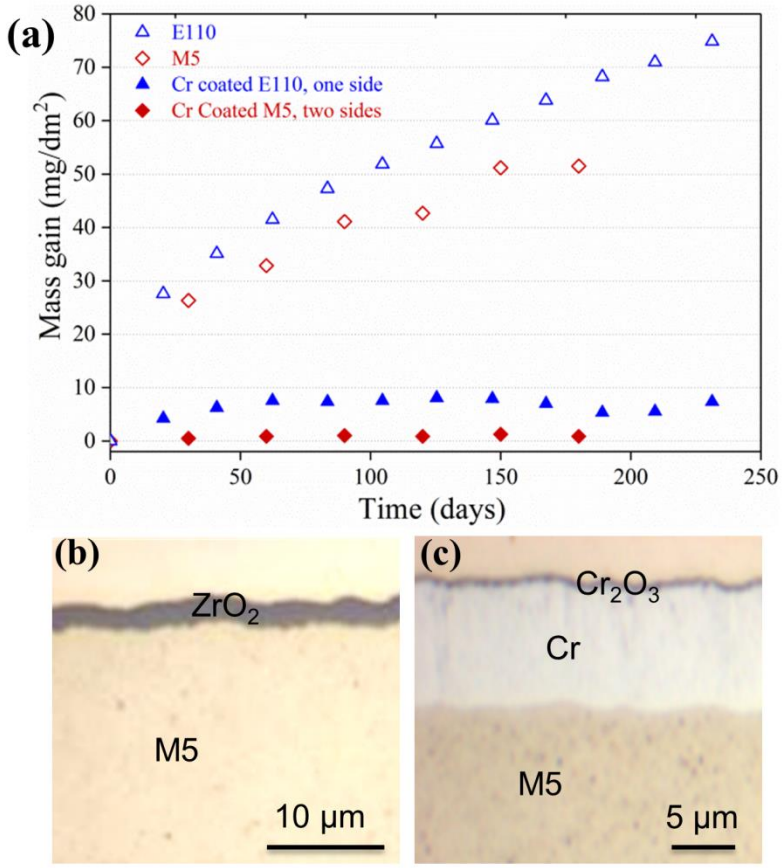

Figure 3 *Comparison of mass gain and oxide scale thickness between uncoated and PVD Cr-coated Zr alloys after hydrothermal corrosion in autoclave testing. (a) Mass gain rate, M5: PWR water chemistry at 360°C, 18.7 MPa and E110: WWER environment at 360°C, 19.7 MPa; cross-sectional metallographic observations of (b) uncoated and (c) Cr coated M5 after exposure for 60 days.* [27,48]

During fuel rod insertion and fuel assembling, surface coatings may be scratched or scraped away locally. Coating technology thus should demonstrate that any defects, like cracking or spallation, in the coatings do not negatively affect the benefits of the coating or the performances of the underlying substrate (for instance the bimetallic effect via exposed interfaces accelerating the corrosion rate of the substrate [93]). Brachet et al. investigated the impact of pre-existing defects (i.e. cracks in as-deposited coatings) on the corrosion performance of PVD Cr coatings on M5 [27]. After autoclave testing under PWR conditions for 60 days, as shown in **Figure 4**, the cracks had only a limited and localized impact without spallation of the coatings or accelerated corrosion of the underlying Zr alloy substrate. Nevertheless, longer exposures, at least up to one refueling cycle, are still required to verify the findings.

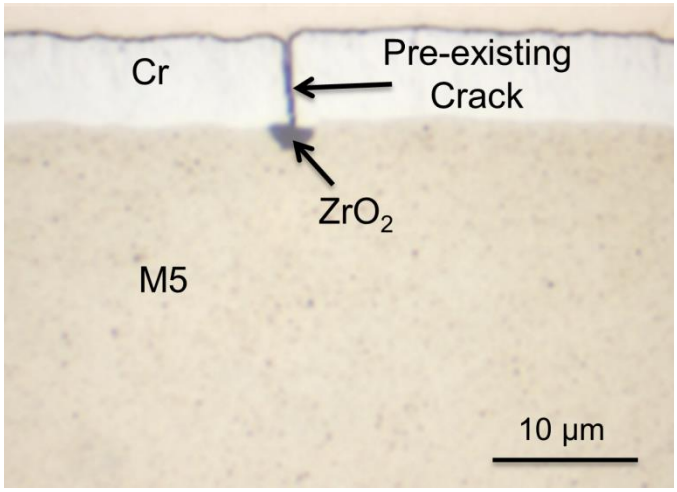

Figure 4 *Cross-sectional micrograph of PVD Cr-coated M5 with a pre-existing crack through the coating after autoclave testing for 60 days.* [27]

CrAl alloy: **Figure 5** compares the weight gain and oxide scale thickness between uncoated and PVD CrAl (15 wt.% Al) coated Zircaloy-4 tested in PWR conditions [85]. After exposure for 240 days, a homogeneous oxide layer of less than 1 µm consisting of 35 at.% oxygen, 7 at.% aluminum and 58 at.% chromium grew on CrAl coatings. In comparison, a ~4 µm cracked oxide layer formed on the uncoated, inner side of the Zircaloy-4 tube. Formation of low-Al $(Cr, Al)_2O_3$ solid solution may inhibit dissolution of the Al during hydrothermal corrosion of the CrAl (15 wt.% Al) alloy [94].

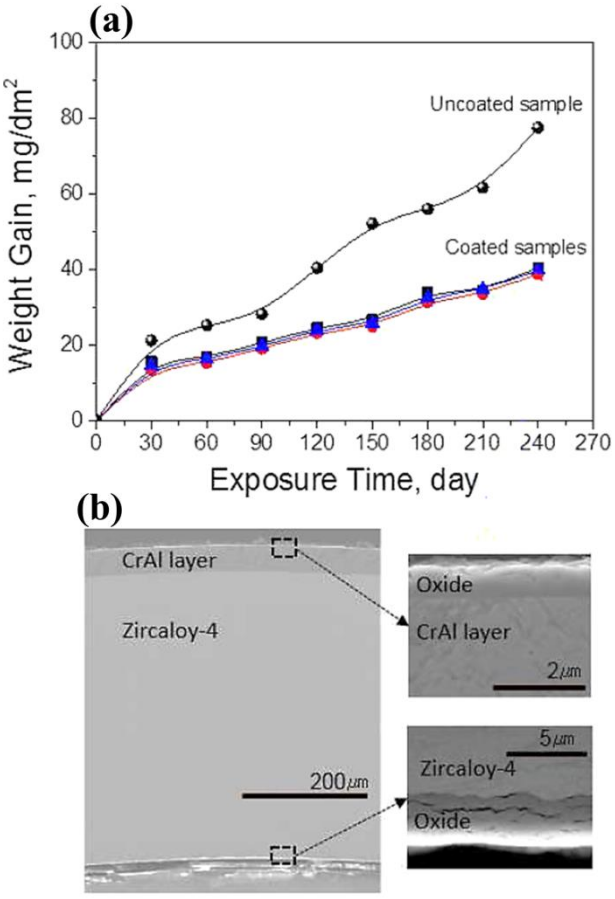

Figure 5 *Comparison of (a) weight gain and (b) oxide scale thickness (240 days) between uncoated and PVD CrAl (15 wt.% Al) coated Zircaloy-4 in PWR simulation loop condition at 360°C and 18.9 MPa.* [85]

FeCrAl alloy: FeCrAl alloys have been proposed as protective coatings considering their exceptional oxidation resistance arising from selective oxidation of Al at elevated temperatures. Hydrothermal corrosion tests in autoclaves revealed that both FeCrAl bulk and coatings possess good corrosion resistance via growth of primarily spinel-type oxides consisting of Fe and Cr [95–97], as displayed in **Figure 6**. In the case of coatings, a transition layer (Fe- or Cr- based oxide phases) grew inwardly between the spinel oxide layer and the FeCrAl layer. Long-term exposure of bulk FeCrAl alloys found dissolution of the Fe-rich spinel oxides in hydrogen water chemistry. Overall, the thickness loss rate, a maximum ~2 μm after one year in the absence of irradiation, is inconsequential with regard to the thick cladding. However, in case of thin coatings the dissolution rate and associated microstructure evolution during long-term exposure needs to be assessed.

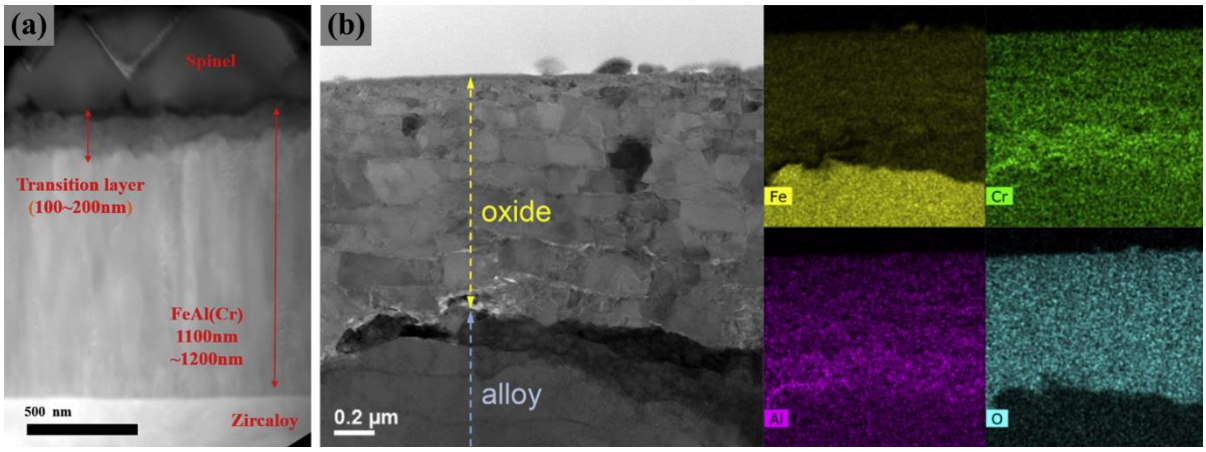

Figure 6 *Cross-sectional images of (a) Fe4Cr34Al (at.%) coating on Zr alloy after exposure at 288°C and 9.5 MPa, BWR condition for 20 days, (b) bulk Fe10Cr5Al (wt.%) alloy after one year of immersion at 330°C and 15 MPa, PWR condition with EDS mapping.* [96,97]

Zirconium Silicides: Zirconium silicides with different stoichiometries (Zr_2Si, ZrSi, and $ZrSi_2$) have been proposed as protective coatings on Zr alloys and the hydrothermal corrosion behavior of $ZrSi_2$ bulk and coating was reported [98–102]. **Figure 7** shows images of bulk $ZrSi_2$ and $ZrSi_2$ coatings on Zr alloy substrate after autoclave exposures at 400°C and 10.3 MPa for 72 h. The corroded bulk $ZrSi_2$ surface revealed cracks and pores, attributed to selective leaching out of Si during exposure. Similar findings were confirmed for the $ZrSi_2$ coatings, which exhibited significant recession and developed a porous and delaminated ZrO_2 surface layer. The hydrothermal corrosion performance of $ZrSi_2$ is not adequate.

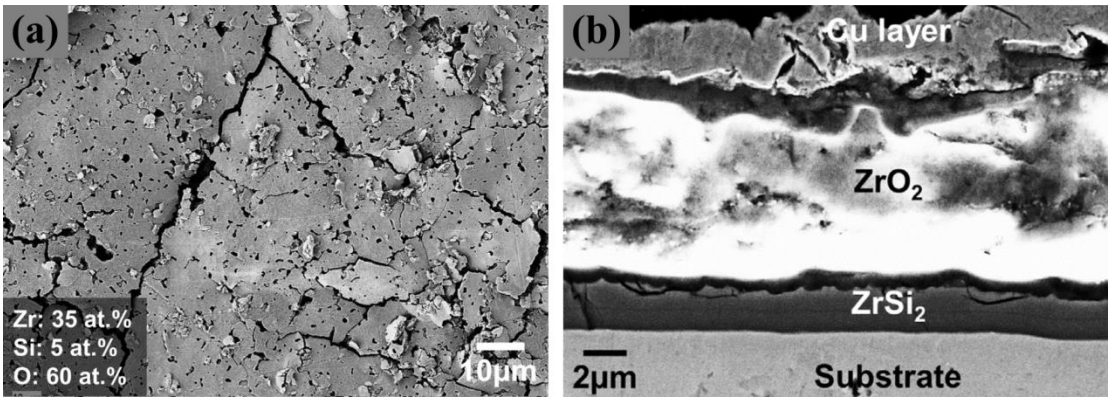

Figure 7 *Hydrothermal corrosion behaviors of $ZrSi_2$ bulk and coating. (a) Surface image of bulk $ZrSi_2$ and (b) cross-sectional image of $ZrSi_2$ coating on Zr alloy substrate after autoclave test at 400°C and 10.3 MPa for 72 h.* [98]

AlCrMoNbZr alloy: An AlCrMoNbZr high-entropy alloy with nearly equal molar ratios was investigated as a protective coating on Zr alloys [57]. The magnetron sputtered coating was composed of a composite of amorphous and bcc-structured nanocrystals. After autoclave corrosion at 360°C and 18.7 MPa for 30 days, a

protective oxide layer based on ZrO_2 and Cr_2O_3 was observed while significant loss of Al from the coatings was confirmed, as shown in **Figure 8**.

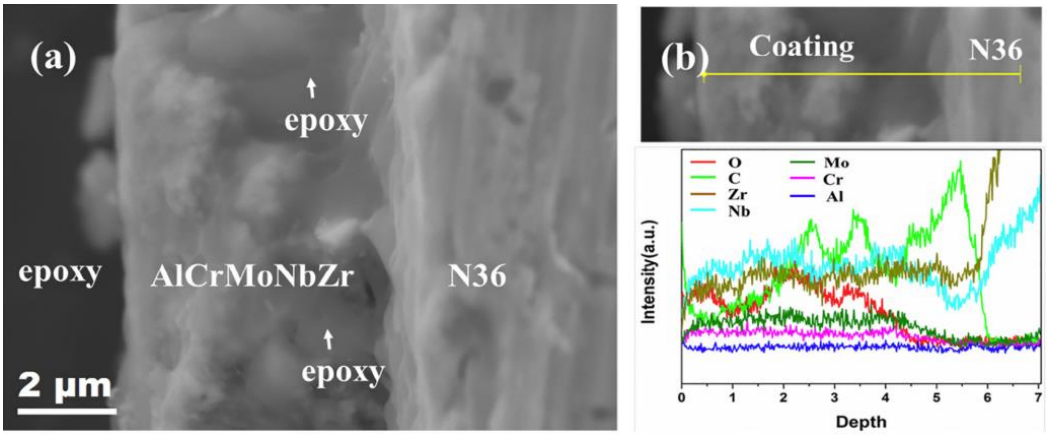

Figure 8 *Autoclave corrosion of the AlCrMoNbZr HEA coating on Zr alloy. (a) Cross-sectional image and (b) EDS line-scan after testing at 360°C and 18.7 MPa for 30 days.* [57]

4.1.2 Ceramic coatings

Oxides: As aforementioned, Al_2O_3 coatings [17,92] are not stable and undergo rapid hydrothermal dissolution under normal operating conditions as demonstrated by several studies. Cr_2O_3 [103] and ZrO_2 [83] coatings, although not investigated, should be stable and exhibit good hydrothermal corrosion resistance based on existing Pourbaix diagrams **(Figure 2).**

C: Nanocrystalline diamond (NCD) coatings deposited by CVD were proposed to enhance the corrosion and oxidation resistance of Zr alloys [77,78]. After long-term exposure at 360°C and 16 MPa for up to 195 days, the coatings maintained their integrity and thicker NCD layers provided stronger protection of the substrate against hydrothermal corrosion and hydrogen uptake. The weight gain of the coated samples was decreased by 35–55% and the hydrogen uptake of the coated samples also decreased significantly.

Carbides: SiC coatings proved to be unstable during autoclave tests simulating normal operations due to Si oxidation and rapid dissolution of SiO_2 [76], similar to other Si-containing coatings. Thus, Si-containing materials [104,105] need proper design in ATF coating applications to avoid selective leaching of Si which can cause fast recession of the coatings during normal operations. The hydrothermal corrosion performances of other carbides (CrC and ZrAlC) coatings were not investigated and reported yet [21,106,107].

Nitrides: Transition metal nitrides are nowadays commercialized as hard protective coatings especially in the tooling industry. Two primary types of nitrides (TiN and CrN) [19,62,63,108–112] are being investigated as protective coatings on Zr alloys. By incorporation of Al, coatings with better high-temperature oxidation resistance can

be obtained [113–115]. Superior hydrothermal corrosion resistance of binary TiN and CrN coatings was observed during corrosion testing in autoclaves [62,115]. Furthermore, the coatings substantially reduced the hydrogen pickup by the Zr alloy substrate. However, the ternary TiAlN and CrAlN coatings demonstrated fast recession again due to rapid, selective dissolution of Al during exposure. One example is presented in **Figure 9**, showing precipitation of AlO(OH) and significant depletion of Al in a TiAlN coating after just 3 days exposure. In comparison, uniform corrosion of TiN coating with a very thin oxide layer was observed. Multilayer coating concepts are being developed to resolve this issue [65].

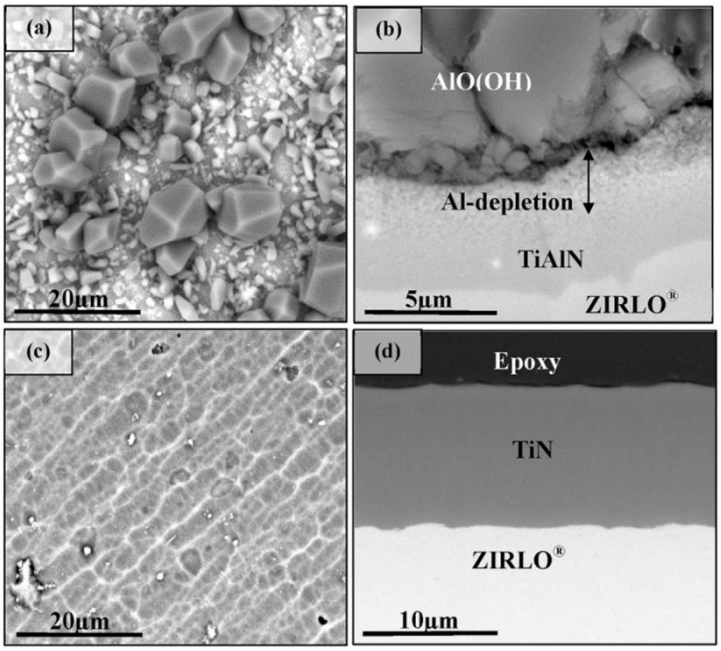

Figure 9 *Surface and cross-sectional images of coated ZIRLO samples after testing at 360°C and 18.7 MPa for 3 days; (a) and (b) TiAlN coating, (c) and (d) TiN coating.* [65]

MAX phases: Several alumina-forming MAX phases are interesting coating materials for the ATF application given their exceptional properties and excellent oxidation resistance as bulk materials [116–123].However, their hydrothermal corrosion performance is seldom investigated. **Figure 10** shows Cr_2AlC coated Zr alloys after autoclave testing at 360°C and 18.8 MPa for 3 days. Parallel micro-cracks existed within the Cr_2AlC coating layer initially owing to the high thermal expansion coefficient mismatch between the coating and the substrate. The Cr_2AlC coating exhibited good corrosion resistance with no visible oxide layer and no depletion of Al, even at regions nearby the micro-cracks. Similar findings have been obtained during autoclave testing of bulk MAX phases Ti_3SiC_2, Ti_3AlC_2, Ti_2AlC and Cr_2AlC for a longer period, 28 days, at 300°C and 12 MPa. No obvious change of the Cr_2AlC sample was found and the superior performance of Cr_2AlC could be attributed to the high Cr content allowing the formation of a passive chromia layer, thus inhibiting preferential removal of Al and further corrosion [124]. The other Ti-based MAX phases cannot form a passivating oxide layer in conjunction with preferential A-layer (Al or Si) dissolution [124]. These findings suggest that Cr_2AlC represents an

attractive option for ATF coating applications. Long-term autoclave tests are still required.

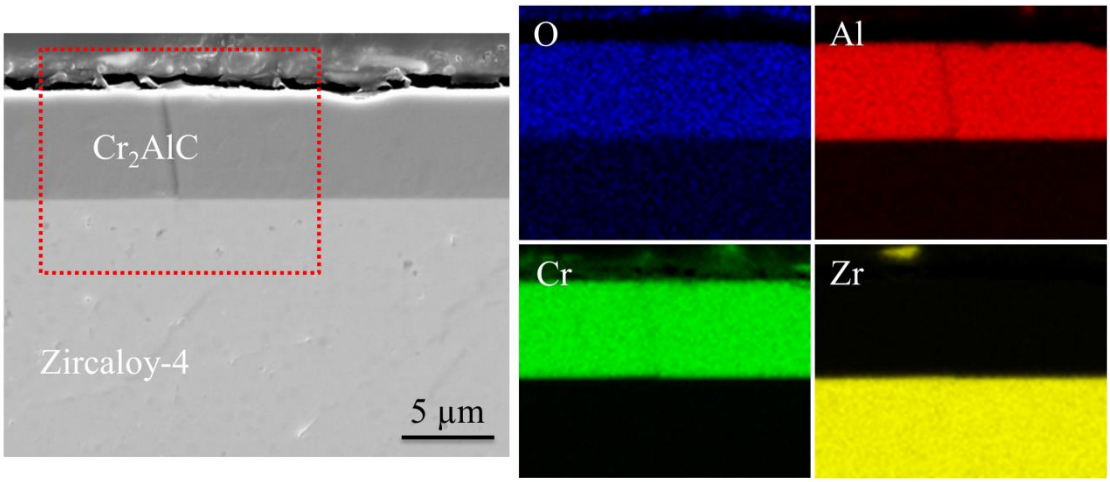

Figure 10 *Cross-sectional image and EDS mapping at the rectangular area of Cr_2AlC coated Zr alloys after autoclave testing at 360°C and 18.8 MPa for 3 days. An initial crack existed due to the high thermal expansion coefficient mismatch between the coating and the substrate.*

4.1.3 Multilayer coatings

Hydrothermal corrosion performances of some multilayer coating concepts have been investigated, especially those targeting to prevent the rapid dissolution of Al or Si during normal operations. Wiklund et al. have deposited Ti/TiN multilayer coatings on Zr alloys and the coatings demonstrated considerably enhanced corrosion and hydriding resistance during autoclave test at 360°C and 22 MPa for 200 days. A thick multilayer coating with numerous sublayers has proved favorable for optimal performance [18]. As indicated earlier, many single-layer Al-containing coatings sustain quick failure via preferential dissolution of Al during hydrothermal corrosion. TiAlN/TiN [65], CrAl/Cr [125] and AlCrMoNbZr/(AlCrMoNbZr)N [126,127] multilayer structures have proven that the top layer can effectively stop Al migration and prevent boehmite phase formation during autoclave tests. **Figure 11** shows a cross-sectional view and corresponding EDS line scan of a TiAlN/TiN multilayer coating on a Zr alloy after autoclave testing as an example. The coatings, with a thin layer of TiN (~1 μm) as a barrier on the surface, showed minimal weight gain, superficial oxygen penetration and no boehmite phase formation [65]. The bi-layered $ZrSi_2/Zr_2Si$ coating concept was proposed to stabilize the Si during autoclave testing [98]. However, the coating was fully oxidized after exposure at 400°C and 10.3 MPa for 72 h.

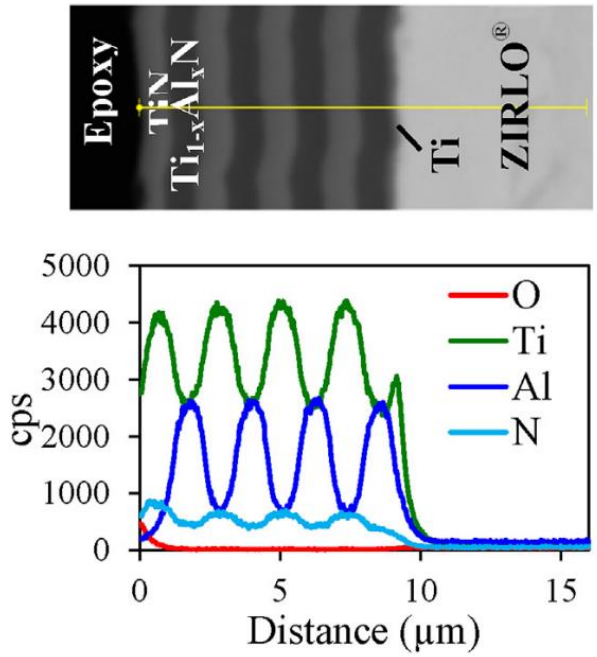

Figure 11 *Cross-sectional image and EDS line-scan of TiAlN/TiN coated Zr alloy after autoclave test at 360°C and 18.7 MPa for 33 days.* [65]

4.2 Mechanical properties

The mechanical properties of the coated claddings, especially their mechanical behavior during in-pile irradiation, are moreover particularly vital to enable their successful implementation [128]. Even though some separate-effect irradiation tests have been conducted and test/verification of lead test fuel rods (Cr coated) in research or commercial reactors are currently under way, no specific analyses of the mechanical behavior of coated claddings after irradiation have been reported yet. This section will summarize the available out-of-pile results concerning the mechanical properties of various coated cladding concepts without irradiation.

The surface mechanical properties of the coated claddings are expected to be improved considering the typical low thickness and specific microstructural features (like small grain size and unique stress state) of coatings. In other words, the coatings are normally harder that the Zr alloy substrates. The fretting and wear damage (grid-to-rod fretting and debris fretting) resistances thus can be enhanced compared to uncoated substrates during normal operations. For instance, PVD Cr [44,45,51] and CrAl [129] coatings have demonstrated significantly improved wear resistance during grid-sliding test and debris wear test; one example is shown in **Figure 12**. Similarly improved fretting-damage resistance was also reported for ceramic coatings, like TiN [19]. However, brittle cracking and fracture were initiated before destroying the TiN coatings owing to its low toughness.

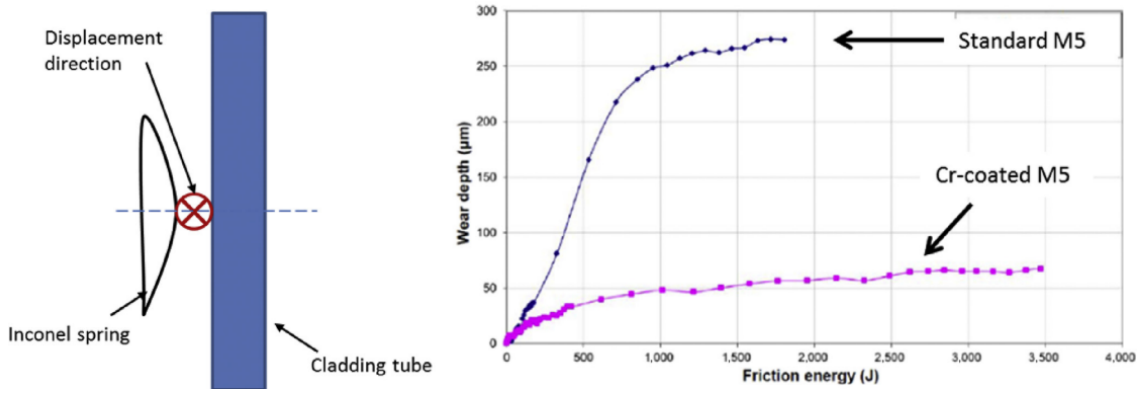

Figure 12 *Schematic representation of the experimental setup for the wear tests and comparison of total wear depth as a function of friction energy of uncoated and Cr coated M5.* [51]

The bulk mechanical properties (like tensile, compression, elongation, creep, etc.) of the coated cladding should be comparable to the uncoated cladding if the coating thickness is sufficiently thin and the deposition/fabrication process does not change the Zr alloy microstructure. This is normally the case for thin coatings deposited by PVD at low temperature. However, for thick coatings deposited for instance by cold spraying, the microstructure and mechanical behavior of the substrate may possibly be modified.

Figure 13 shows an example of the stress-strain curves for PVD Cr-coated M5 and reference uncoated M5 tested at room temperature and 400°C [29]. The curves demonstrated similar mechanical behavior for both samples. Intensive investigations performed on Framatome's PVD Cr coating concept proved that the mechanical properties (yield strength 0.2%, ultimate tensile strength, and total elongation) of the Cr-coated samples all fell within the range of scatter from uncoated samples [29,45]. Similar mechanical properties were also achieved between Cr coated claddings via laser [26] or cold spraying processes [32] and uncoated reference samples. Peeling or spalling phenomena were not observed during ring compression and ring tensile tests of laser coatings and during tensile tests of cold spray coatings. The strength of the Cr-coated samples via laser processing was higher relative to the uncoated reference samples. Furthermore, as displayed in **Figure 14**, the Cr layer demonstrated high adherence and good ductility, maintained a sound microstructure at up to 4% strain, whereas lateral cracks were formed after reaching 6% strain during ring tensile tests [26]. The total elongation at room temperature of the Cr-coated samples (18.5%) via cold spraying was lower than that of uncoated reference tubes (23.0%), but comfortably maintained the current minimum specified for cladding material (15%) [32].

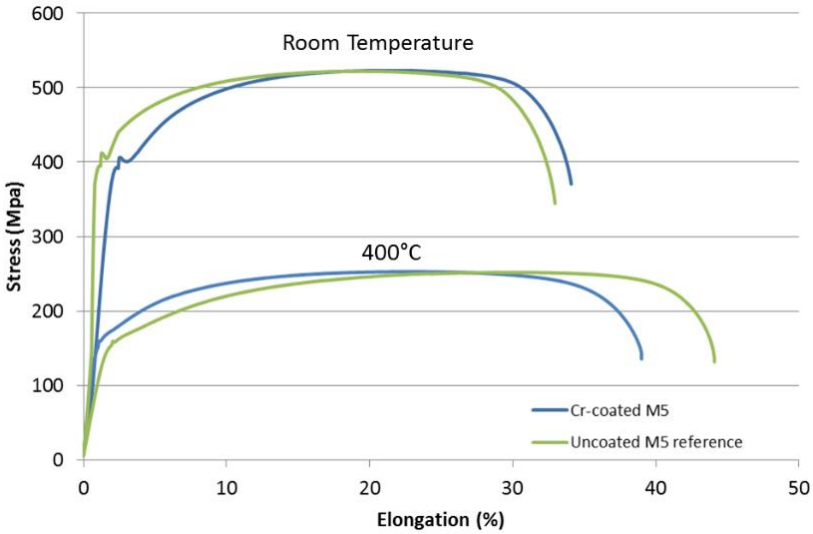

Figure 13 *Tensile tests at room temperature and 400°C of PVD Cr-coated M5 compared to uncoated reference M5.* [29]

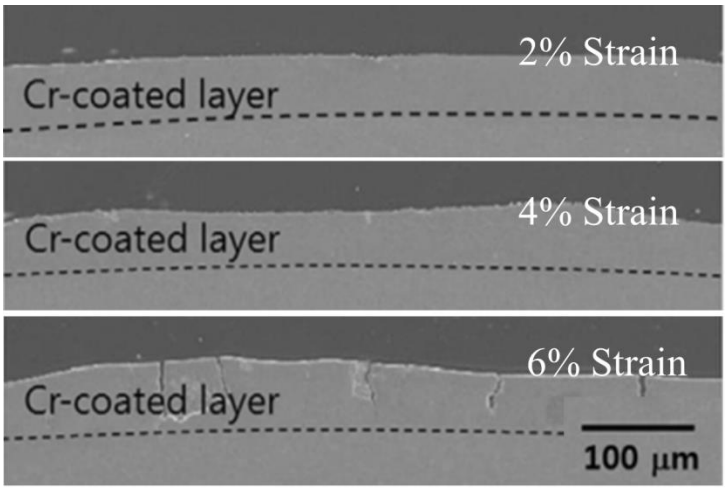

Figure 14 *Cross-sectional observations of Cr-coated Zircaloy-4 cladding tubes after ring tensile tests at 2%, 4%, and 6% strain. Coatings were deposited by a laser process.* [26]

Some detrimental effects of coated claddings on mechanical behavior were occasionally observed especially for coatings deposited by the cold spraying process. The cold spraying process involves strong impact of the substrate via high velocity sprayed particles and significant plastic deformation of deposited coating particles [73]. Ševecek et al. investigated the fatigue behavior of cold sprayed Cr coated cladding and found that environmentally-induced cracks might initiate earlier for coated samples compared to uncoated reference samples in BWR-NWC condition. The premature crack initiation likely connects with the high-level of residual stress and stress concentration in the coating attributable to the inhomogeneities created by the cold spraying process [47]. Investigation of mechanical behavior of a Zr alloy coated with a FeCrAl/Mo (Mo as a diffusion barrier) layer deposited by cold spraying revealed enhanced hardness and cleavage fracture morphology of the Zr matrix

directly below the Mo/Zr interface, which indicated the occurrence of localized deformation owing to Mo particle impact [74].

There is scarce information concerning the mechanical behavior of ceramic-based coatings on Zr alloy substrates. Nieuwenhove et al. reported that micro-cracks appear in a CrN coating at a strain level of about 1.5% [11]. Micro-tensile testing of TiAlN-coated Zr alloys found that transverse cracks within the coating layer start to appear at a strain level of 0.84% [113]. Clearly, these values are much lower than that mentioned before for pure metallic Cr coatings (~6%). Ceramic coatings typically exhibit brittle characteristics and low toughness and thus are more prone to undergo damages like cracking and fracture.

4.3 Irradiation performance

The structural integrity of the coating-substrate system will be highly challenged in the reactor core especially towards high fuel burnup considering well-known irradiation-induced degradation phenomena [128,130]. Depending on the operational temperatures and damage levels, mainly five irradiation-induced degradation mechanisms exist for materials (i.e. irradiation hardening and embrittlement, phase instabilities, irradiation creep, volumetric swelling and He embrittlement) [131]. The coating and substrate regularly behave differently under irradiation owing to mismatches of their fundamental physical properties, such as strain mismatches in irradiation-induced growth and creep [128]. Additionally, the interfaces between dissimilar crystal structures with different lattice parameters are energetically favorable sinks for growth and aggregation of defect clusters. The hydrothermal corrosion or dissolution rate can be enhanced under irradiation conditions. Thus, the hydrothermal corrosion behavior of the coating-substrate system as well as the chemical and mechanical compatibility between the coating and the substrate under irradiation (in-pile) conditions needs thorough assessment and validation.

4.3.1 Out-of-pile behavior

Preliminary ion irradiation experiments were performed on some relatively mature coating concepts (mainly Cr-based) to simulate neutron-induced damage.

The interface structure and interface stability of a PVD Cr coated Zr alloy under irradiation were examined with damage at the interface of 10 dpa (displacements-per-atom) using 20 MeV Kr^{8+} ions [33,34]. The results indicated primary coherent or semi-coherent crystallographic relationships of the Cr-Zr interface ensuring the adhesive strength of the coating. After irradiation, good chemical and microstructural stability of the Zr/Cr interface was confirmed without degradation of the interface and irradiation-induced diffusion of Cr into the substrate. The adhesion of the Cr coating to Zr substrate did not decrease after this specific ion

irradiation. Irradiation of vacuum arc Cr coatings by 1.4 MeV argon ions to 25 dpa indicated radiation-induced isotropic growth of grains with formation of vacancy voids and radiation-induced swelling within the coatings [38]. Nevertheless, the swelling was observed at a low level (0.66 %), demonstrating a high irradiation resistance of the chromium coatings. Maier et al. have examined the irradiation tolerance of cold sprayed Cr coatings via *in-situ* TEM using 1 MeV Kr^{+2} ions to 3 dpa [35]. Radiation-induced defects, such as black spots and dislocation loops, were observed. They suggested that the severely plastically deformed microstructure of the cold sprayed Cr delayed the onset and growth of radiation-induced defects.

Kratochvílová et al. have investigated the irradiation tolerance of a CVD polycrystalline diamond coating on Zr alloy substrate using 3 MeV Fe^{2+} to 10 dpa [132]. After ion beam irradiation, the film did not reveal any microstructural changes and showed satisfactory structural integrity.

Energetic particle irradiation of TiN coatings using 134 keV Xe^{+} ions at 473 K to 6.2 dpa revealed significant microstructural alterations with radiation-induced segregation of the coatings (TiN is prone to dissociate creating Ti-enriched zones) [110]. The nucleation and growth of Xe bubbles were believed to play a key role in its dissociation behavior. It is suggested that nanocrystalline TiN thin films may not be a suitable solution as protective coatings on Zr-based alloys.

Bugnet et al. investigated the ion irradiation of Cr_2AlC and Cr_2GeC coatings deposited on sapphire substrates with 320 keV Xe^{2+} focusing on single grains [133]. The results indicated that both compounds were amorphized at moderate fluence rates. Annealed of cold spraying Ti_2AlC coating on Zr alloy substrate up to 923 K resulted in formation of three interfacial intermetallic compounds ($ZrAl_2$, ZrAl, and Zr_3Al). Ion irradiation to a damage level of 100 peak dpa disrupted the layered structure of the Ti_2AlC coating while amorphization was observed for some of the intermetallic compounds together with hardening effect [134]. V_2AlC coatings deposited by magnetron sputtering on Zr substrate were irradiated using 500 keV He ions [119]. The results showed that the He bubbles preferentially nucleated along the substrate-coating interface and resulted in reduced adhesion strength of the V_2AlC coating. Thus, optimizing the interfacial structure is of substantial importance for improving the irradiation resistance of the coating-cladding system.

The interface stability and mechanical properties of AlCrMoNbZr/(AlCrMoNbZr)N multilayer coatings with individual layer thickness of 5 nm, 10 nm and 50 nm, subjected to helium ion irradiations were studied [127]. He ion irradiation induced intermixing and chemical reactivity was observed in case of coating with lower modulation periods. Nanoindentation tests revealed decreased hardness of all multilayer coatings mainly due to the thermal effect caused by irradiation.

The irradiation resistance of other coating concepts is largely unexplored yet. The irradiation performance of some intensively investigated coating materials, like FeCrAl alloys and MAX phases, have been examined in bulk form, which can provide some glimpse of their behavior when applied as protective coatings. FeCrAl alloys with a high Cr addition are vulnerable to irradiation hardening and embrittlement, plus phase instabilities owing to the formation of Cr-rich α′ precipitates [135,136]. MAX phase materials generally exhibit strong tolerance to energetic ion and neutron irradiation damage [137]. However, different behaviors were seen experimentally. Irradiation-induced damages, like phase transition and amorphization, cracking and surface exfoliation, were sometimes observed [138–141]. Thus, the behavior of FeCrAl and MAX phase coated Zr alloy systems under irradiation needs to be adequately addressed in the future.

4.3.2 In-pile behavior

A five-year irradiation program was launched in 2016 to test the in-pile behavior of PVD Cr-coated (Framatome) zirconium alloys (plus SiC_f/SiC composites) in the Gösgen nuclear power plant (PWR) in Switzerland [46]. Visual inspection after one cycle (one-year irradiation and corrosion) proved that the Cr coatings were very stable without indications of delamination. The Cr-layer showed essentially the same degree of homogeneity as before irradiation and a golden color corresponding to growth of a very thin Cr-oxide layer. Lead test rods (LTRs) of cold sprayed Cr coated claddings in commercial reactors led by Westinghouse are planned in spring 2019 [142].

Irradiation campaigns of CrN, TiAlN and CrAlN coatings on Zr alloys have been conducted in the Halden Reactor (Norway) [143]. Only the CrN coating survived and remained to a large extent (>80 %) intact after exposure; both the TiAlN and CrAlN coatings disappeared from the fuel rod surface related to the rapid selective dissolution of Al. Some degree of damage corresponded to cracking and localized delamination of the CrN coating occurred, likely because of mechanical problems which led to overheating of the fuel-rod cladding. Zirconium oxide grew beneath the areas where the coatings were damaged, as shown in **Figure 15**, confirming the loss of protectiveness in these areas.

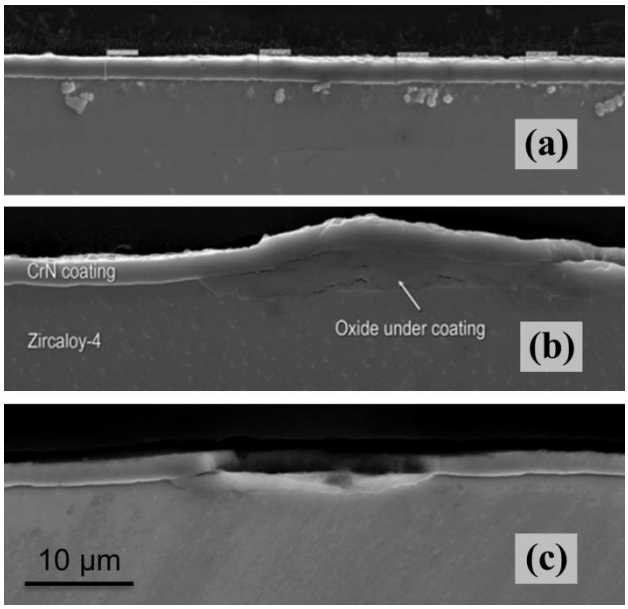

Figure 15 *Cross-sectional images of CrN-coated Zr alloy tube before (a) and after (b, c) irradiation in the Halden Reactor for 287 days. Zirconium oxide formed under cracked and delaminated coating areas.* [143]

4.5 Other property requirements

Coating solutions need to demonstrate compatibility with welding using current processes for bare Zr alloy fuel cladding. The welding performance of PVD Cr and CrAl coated claddings has been examined [48,51,85]. Welded specimens also have been subjected to hydrothermal corrosion. Using the current resistance welding process, Bischoff et al. have shown welding of the Cr coated tube without modifying the welding process [51]. Localized spallation of the Cr coatings near the welding zone was reported by Krejci et al. after autoclave exposure for 210 days in WWER conditions using tungsten inert gas (TIG) welding [48]. The CrAl-coated cladding bonded well to the end cap without peeling or damage of the coating layer after friction welding and corrosion for 120 days in a PWR simulation loop [85].

The impact of a coating on surface wettability and heat transfer of the cladding tube has been infrequently investigated. Pure Cr coatings demonstrate a slightly higher contact angle with static water droplets compared to fresh Zr alloy surfaces [103,144]. A much higher contact angle was seen for AlCrMoNbZr-based coatings [57] and a lower contact angle was measured for $ZrSi_2$ coatings [101]. Enhanced wettability was observed after oxidation or after gamma irradiation of Cr coatings and for Cr_2O_3 coatings [36,145]. Increased wettability and porosity of the coating layer could improve the heat transfer characteristics of the fuel cladding [103,144].

5 Performance under accident scenarios

The anticipated key performance features of innovative ATF claddings for improved safety margins and increased coping time during accident scenarios are reduced oxidation kinetics in high-temperature steam/air with simultaneously minimized hydrogen generation and enthalpy input, together with improved strength to maintain core coolability and retain fission products [4]. High-temperature oxidation resistance of materials relies on the growth of a thermodynamically stable oxide layer acting as a physical diffusion barrier between the reactant phases. The oxidation kinetics are determined by the chemical nature of the transport processes within the oxide scale. **Figure 16** shows the parabolic oxidation rates for various scale-forming bulk materials in steam as a function of temperature [7]. It can clearly be seen that robust oxide scales for protecting the underlying matrix from fast consumption at elevated temperatures are those made of chromia, alumina or silica. Their growth rates decrease following the aforementioned sequential order. Even though chromia and silica can form volatile suboxides (in oxygen) or hydroxides (in steam) at elevated temperatures, their volatilization rates are normally sluggish in low-speed flow environments [146]. The other oxide scales, such as FeO_x, ZrO_2, NiO or TiO_2, are featured by much higher growth rates at elevated temperatures [147].

The oxidation mechanisms and degradation phenomena of oxidation-resistant coatings are essentially similar to bulk materials. Coating concepts not containing Cr, Al, or Si should not be suitable for ATF applications. However, additional constraints appear with coatings, mainly chemical and mechanical compatibility with the substrate, which may remarkably restrict their performance. Since coatings are normally thin, they contain a limited reservoir of the scale-forming element. Thus, interdiffusion/reaction between the coating and the substrate can deplete the scale-forming elements and introduce undesirable elements into both the coating and the substrate, deteriorating their oxidation resistance. Mechanical constraints, largely arising from thermal expansion mismatch, can also lead to premature degradation of the coating, such as by cracking and delamination. The mechanical properties (like ballooning, burst and fracture resistance, post-quench residual strength and ductility) of coated claddings are normally improved assuming reduced oxidation kinetics at LOCA relevant temperatures (below coating-substrate eutectic temperature). The performances of various coated cladding concepts during severe accidents have rarely been studied yet and, as-expected, are exceedingly challenging.

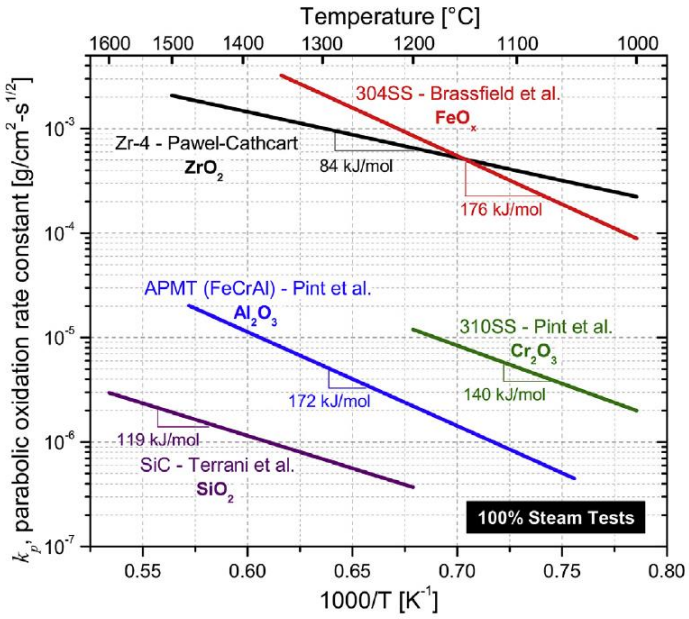

Figure 16 *Parabolic oxidation rates for various scale-forming materials in steam as a function of temperature.* [7]

5.1 Design-basis accidents

5.1.1 Metallic coatings

Oxidation of **aluminum**-modified Zr alloy surfaces (synthesized by magnetron sputtering of aluminum and subsequent thermal annealing) at 800°C in steam for 120 min displayed better oxidation resistance with average oxide layer thicknesses of ~0.7 µm (around 8 µm for un-modified specimens). However, the oxide layer was slightly thicker for treated specimens after oxidation at 1000°C [148]. The poor oxidation performance of the coated surfaces is likely attributed to the formation of brittle intermetallics (see calculated phase diagram of Zr-Al in **Figure 17**; Zr-Cr, Zr-Fe and Mo-Zr systems are also given [149]) and surface cracks, preventing the growth of a continuous and uniform alumina scale.

The oxidation performance of thick **Si** coatings (up to 150 µm) fabricated by plasma spray with subsequent laser beam scanning treatment was investigated at 1200°C in steam. [150] The coated samples displayed improved oxidation resistance with ~60% mass gain compared to uncoated ones after exposure for 2000 s. However, here the coatings were too thick and as aforementioned, pure Si is unstable during normal operation.

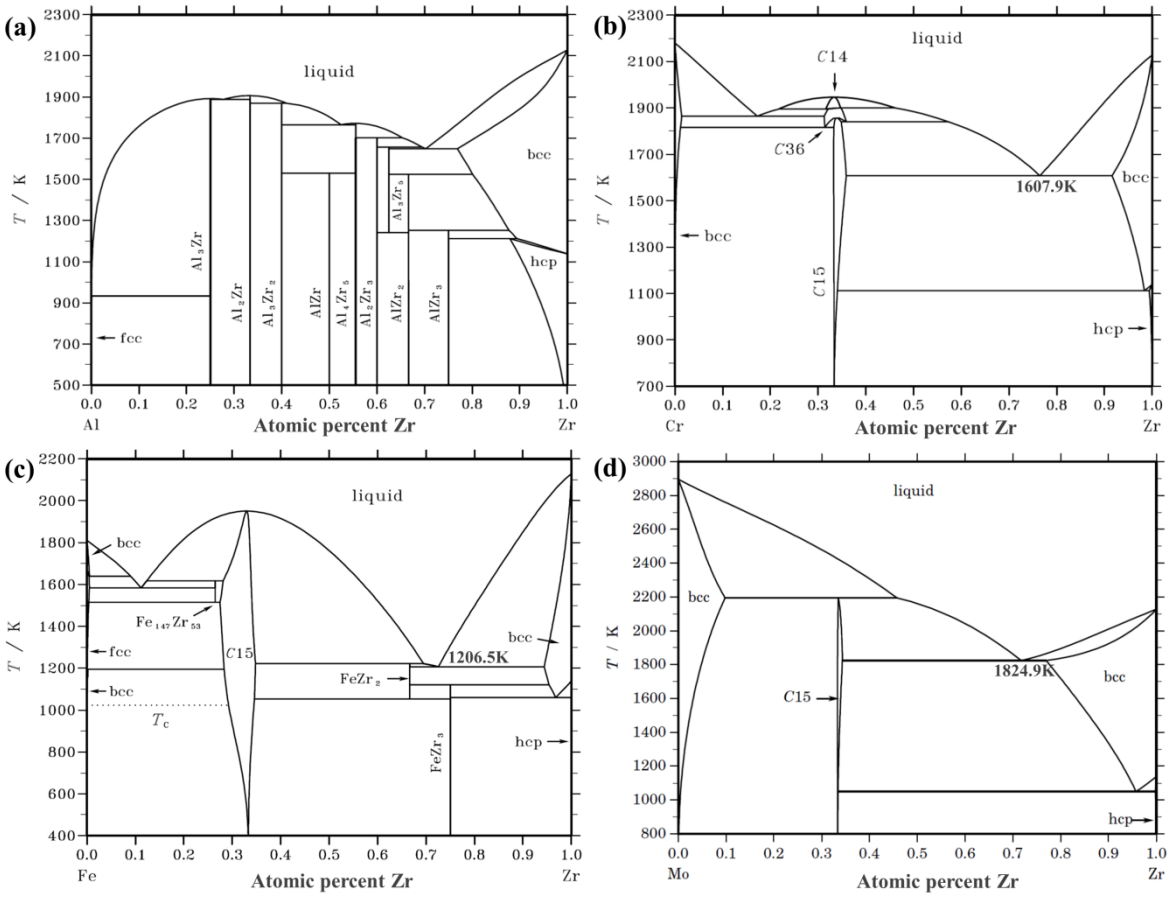

Figure 17 *Calculated phase diagrams of (a) Zr-Al, (b) Zr-Cr, (c) Zr-Fe and (d) Mo-Zr.*

Steam oxidation performance of **Cr** coatings, deposited by diverse methods, have been intensively examined [23,25–29,39,41,42,48–51,53]. Generally, the high-temperature oxidation kinetics of Cr-coated Zr alloys is significantly reduced compared to uncoated alloys up to 1200°C relevant for LOCA scenarios. The coatings form a protective Cr_2O_3 scale during oxidation, demonstrating acceptable performance even under beyond design-basis conditions below the Zr-Cr eutectic temperature (1332°C, as shown in **Figure 17 (b)**). **Figure 18** compares the oxidation performance and mechanical behavior of PVD Cr coated and uncoated Zr alloys. Clearly, the oxide scale thickness on the Cr coating layer is one order of magnitude lower than that on bare Zr alloys during oxidation at 1200°C in steam, **Figure 18** (c). Consumption of the coatings is determined by two combined processes, i.e. surface oxidation and inward diffusion into the substrate, as displayed in **Figure 18** (d). The 12-15 µm Cr coating deposited by PVD can delay the oxidation of the Zr alloy substrate for approximately 5 hour at 1100°C or 1 hour at 1200°C in steam [45]. It is necessary to point out that at high water vapor partial pressure (>10 kPa) formation of volatile chromium oxyhydroxides becomes prominent, which further limits its protective capability to lower temperature (~1040°C) [146]. The Cr-coated samples also demonstrated negligible reduction of residual strength and ductility before the complete consumption of the metallic Cr layer, **Figure 18** (e), and improved ballooning and rupture resistance [26,30,53]. In addition, the chromium coatings revealed high adherence without peeling including at the vicinity of the

burst opening. The amount of hydrogen picked up by the cladding was significantly reduced simultaneously due to the existence of the Cr_2O_3 barrier. Similarly, enhanced oxidation and mechanical performances were reported for Cr coatings fabricated by other methods. However, during long-term scenarios inward diffusion of Cr could cause hardening and enhanced embrittlement of the cladding due to formation of brittle intermetallics [48]. Han et al. found that the completely oxidized Cr coating can be reduced by the Zr substrate, revealing more complicated oxidation mechanisms [56]. In case of cold sprayed coatings, accelerated growth of initially existing cracks and bending of the coated tubes were observed during oxidation [41]. Occurrence of these undesirable features needs to be addressed and avoided via coating optimization in the future.

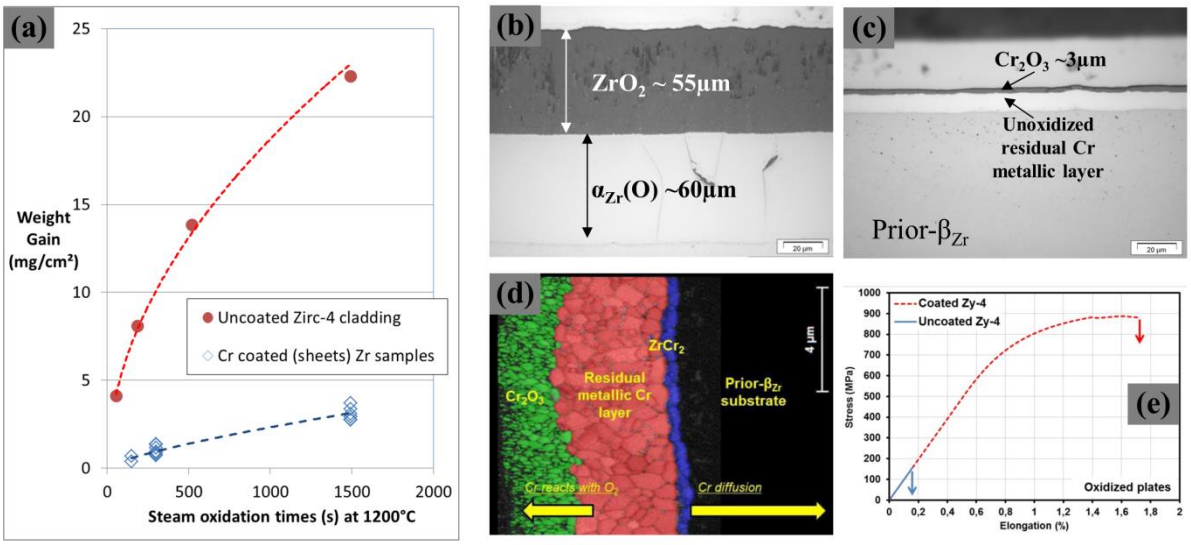

Figure 18 *Comparison of oxidation performance and mechanical behavior between PVD Cr coated and uncoated Zr alloys. (a) oxidation rate, oxide scales on (b) uncoated Zircaloy-4 versus (c) and (d) Cr- coated samples after oxidation at 1200°C for 300 s in steam, (e) tensile stress-strain curves obtained at RT after two-side steam oxidation for 15000 s at 1000°C.* [27,53]

Al- and/or Si-containing Cr alloys such as **CrAl** and **CrAlSi** were also considered as protective coatings, aiming to improve the oxidation resistance relative to pure Cr coatings. A CrAl (30 wt. % Al) coating layer deposited via a laser coating process resulted in significant mixing of CrAl coating metal with the Zr substrate. The coatings demonstrated poor oxidation resistance because of considerable interdiffusion and formation of intermetallic compounds [79]. CrAl coatings deposited by PVD displayed much better oxidation performance. A metastable alumina layer developed on the CrAl coatings with Al composition over 43 at% during oxidation at 700°C in steam [39]. A 1 µm oxide layer (mainly Cr_2O_3) formed on CrAl (15 wt.%)-coated cladding after oxidation at 1200°C for 3000 s in steam and water quenched [85]. Improved rupture resistance and post-quench ductility were also seen for coated samples [85]. Decreased oxidation rates of PVD CrAlSi coated specimens compared to bare Zr alloys up to 1200°C were reported [151]. However, coating constituent elements (primary Al or Si) diffused substantially into the substrate and formed intermetallic phases with the Zr alloy substrate during oxidation.

Alumina-forming **FeCrAl** alloys (adequate addition of Cr and Al) are well known for their excellent high-temperature oxidation resistance and thus have been intensively investigated as protective coatings on Zr alloys. Formation of a protective alumina layer was confirmed during oxidation at relatively low temperature, such as 700°C in steam [96]. However, rapid degradation of the coatings without protection was seen once the oxidation temperature exceeds the Fe-Zr eutectic reaction temperature (around 930°C, **Figure 17 (c)**) [152]. Formation of interfacial intermetallic compounds at lower temperatures also embrittles the coated cladding [153]. Many efforts now attempt to identify a suitable interlayer as diffusion barrier [64,74,82,95,154].

Oxidation of **zirconium silicide** (Zr_2Si, ZrSi, and $ZrSi_2$) coatings revealed that $ZrSi_2$ possesses the best anti-oxidation behavior via formation of an oxide layer consisting of nanocrystalline SiO_2 and $ZrSiO_4$ in an amorphous Zr-Si-O matrix at 700°C in air [100]. However, the coatings have very limited improvement at higher temperatures. The incorporation of ZrO_2 into the scale during oxidation likely compromises the protective nature of the coatings.

5.1.2 Ceramic coatings

Durability of **oxide** coated Zr alloys is largely unexplored, except one study showing that a pre-oxidized ZrO_2 layer significantly enhances breakaway oxidation resistance of the fuel claddings [83]. Even though oxides should be thermodynamically stable (note that volatilization could occur) and act as diffusion barriers at elevated temperatures, additional validation of their physical integrity during oxidation is required.

Oxidation resistance of **polycrystalline diamond** coated cladding was slightly improved at 950°C [77]. Since carbon/carbon composites form gaseous carbon oxides during high-temperature oxidation, and substantial effort has been devoted to develop protective coatings for this category of materials [155], the enhanced oxidation resistance of diamond coatings is expected to work only at low temperatures.

SiC coatings with various concentrations of Si on zircaloy plates showed enhanced oxidation resistance at 900°C in steam attributed to oxidation of the Si component to form a silica layer [105]. Oxidation of Cr-based coatings (Cr and CrC, CrSiC) on the inner side of a Zr alloy tube deposited by DLI-MOCVD revealed that amorphous chromium carbide coatings (up to ~25 μm thick) showed the most promising properties [20,21]. The **CrC coatings** demonstrated good adherence, preserving their integrity after oxidation at 1100°C followed by water quenching. However, some small cracks were evident. In addition, the coatings shifted the catastrophic oxidation of the uncoated alloy substrate towards higher temperatures and delayed its complete oxidation for more than 2 h at 1200°C in steam. Oxidation of PVD

ZrAlC coatings on a Zr alloy substrate indicated no protection effect at temperatures beyond 800°C in steam owing to cracking and formation of a mixed oxide scale (ZrO_2 and Al_2O_3) [107].

Improving the oxidation resistance of **transition metal nitride** (TMN)-based coatings has represented an important topic for many decades with the purpose of increasing the durability and efficiency of cutting tools [156]. Hard TiN protective coatings were initially developed for industrial usage. Their limited oxidation resistance has motivated the continuous evolution toward ternary and quaternary Al-containing TMN (such as TiAlN, CrAlN and CrAlYN) systems with enhanced oxidation performance as well as additional attractive mechanical and chemical properties [156,157]. Mixed oxide scales consisting of both Al_2O_3 and transition metal oxide grow during high-temperature oxidation of these Al-containing nitride coatings. Therefore, CrAlN-based coatings, forming a mixed Cr_2O_3 and Al_2O_3 scale, typically possess better oxidation resistance than TiAlN-based coatings. The incorporation of minor amounts of "reactive" elements (for example Y, Hf, Zr, Yb) can further reduce the oxidation rate and improve scale adhesion [156]. Brova et al. have investigated the oxidation performance of un-doped and ytterbium-doped titanium aluminum nitride (TiAlN, Ti:Al ~1) coatings on Zr alloys [114]. **Figure 19** shows the microstructure of the oxide scale after oxidation at 1000°C for 25 min in air. The coated samples clearly demonstrated improved oxidation resistance at this temperature, with roughly eight times thinner oxide layer on top. Logically, the oxide scale on coatings are composed of both TiO_2 and Al_2O_3, **Figure 19** (b) and (c). However, a large quantity of fine voids was found inside the oxide layer and partial delamination likely occurred at the scale/coating interface. This suggests that an optimized Yb dopant concentration leads to a lower growth rate of oxide scale and improved scale adherence, **Figure 19** (c). Over-doping of Yb will impose adverse effects and worsen the oxidation resistance. Validation of coating performance at higher temperature in a steam atmosphere is needed.

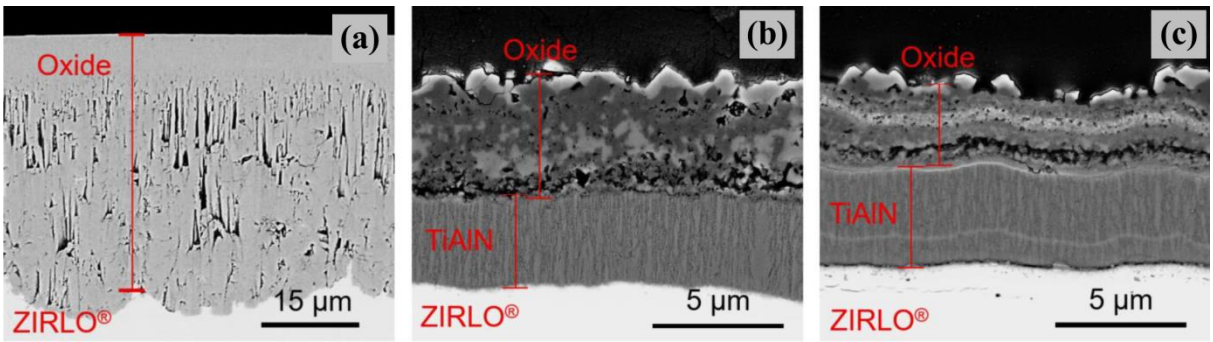

Figure 19 *Cross-sectional SEM-BSE images after oxidation at 1000°C for 25 min, (a) uncoated Zr alloy, (b) TiAlN coated and (c) TiAlN with 0.64 at. % Yb coated.* [114]

Enhanced oxidation performance was also confirmed for other nitride coatings, for instance CrN, CrAlN, TiAlCrN and CrAlSiN, on Zr alloy substrates during oxidation up to at least 1200°C in an air or steam atmosphere [48,112,115,158,159]. However, one

common issue for these hard nitride coatings is that they are susceptible to cracking especially undergoing temperature changes and/or high deformation. One example is shown in **Figure 20**. The rapid growth of Zr oxides beneath the localized cracked coatings can exacerbate the premature failure of the coatings during oxidation.

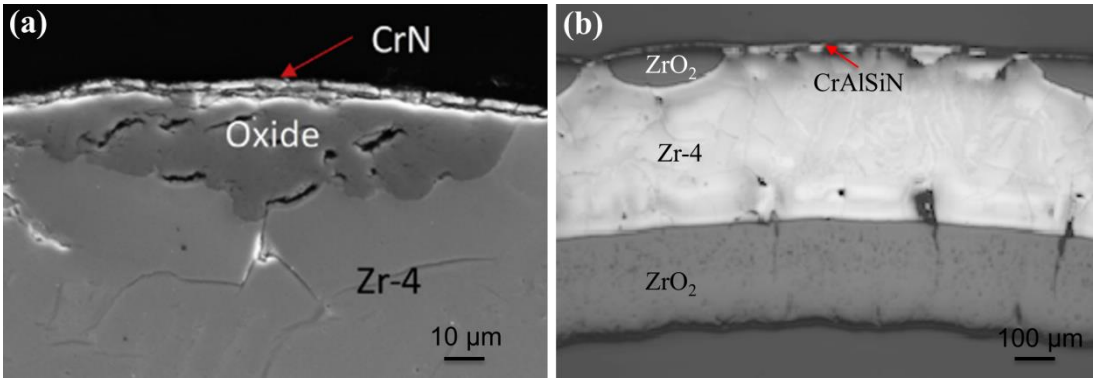

Figure 20 *Cross-sectional images of (a) CrN coating [115] and (b) CrAlSiN coating [158] oxidized at 1100°C in steam for 15 min and 30 min, respectively. Cracking of both coatings with rapid growth of ZrO_2 layer beneath cracks was observed.*

Alumina-forming MAX phases (Ti_2AlC, Ti_3AlC_2 and Cr_2AlC) possess excellent high-temperature oxidation resistance and autonomous self-healing capability [122,160], making them exceedingly promising candidates as protective coatings. The oxidation performance of Ti_2AlC and Cr_2AlC coatings on Zr alloy substrates has been reported. During high-temperature oxidation, thick Ti_2AlC coatings deposited by spraying often cannot establish a dense and continuous alumina layer on top due to their porous structure and many impurities [117]. In the case of thin Ti_2AlC coatings deposited by PVD, improved oxidation resistance was shown at the relatively low temperature of 800°C in steam. However, rapid oxidation with significant cracking and spallation of the coatings occurred once oxidation temperatures reached 1000°C [120]. Growth of layered, mixed oxide scales likely caused the poor performance at elevated temperatures. In comparison, thin Cr_2AlC coatings possess superior oxidation resistance and oxidation-induced self-healing capability via growth of a thin and dense alumina layer during oxidation at 1000°C in steam [87]. **Figure 21** illustrates the microstructure of Ti_2AlC and Cr_2AlC coated Zr alloys via PVD after oxidation at 1000°C in steam. A thick ZrO_2 layer formed on the Ti_2AlC coated sample even after oxidation for just 5 min. A protective alumina layer, ~ 0.6 μm thick (two hundred times thinner than that of ZrO_2 layer formed on uncoated alloy), formed on the Cr_2AlC coating after oxidation for 60 min, **Figure 21** (b). An initial micro-crack within the coating was healed via fast growth of alumina and associated volume expansion. However, during oxidation, rapid diffusion of Al from the MAX phase coatings into the substrate takes place because of the high migration rate of the A-element in the MAX phase structures.

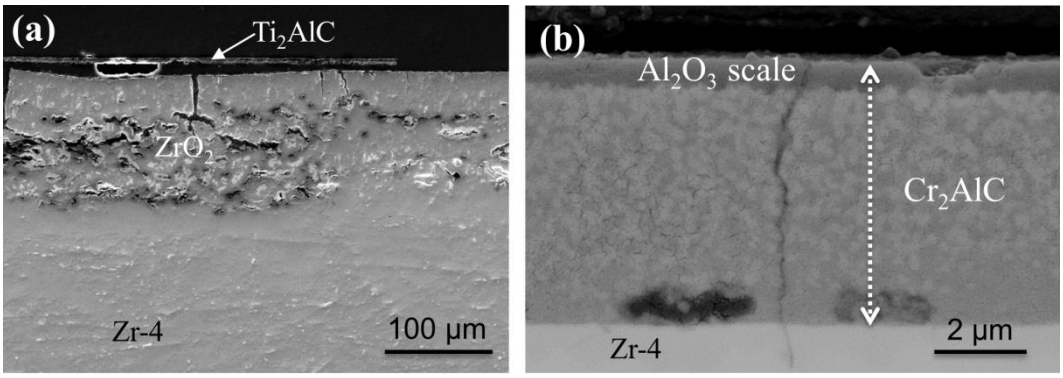

Figure 21 *Cross-sectional images of (a) Ti_2AlC coated [120] and (b) Cr_2AlC coated [123] Zr alloy after oxidation at 1000°C in steam for 5 min and 60 min, respectively.*

5.1.3 Multilayer coatings

Investigations performed to evaluate the oxidation performance of multilayer coatings on Zr alloys mainly focused on verifying the capability of a diffusion barrier to prevent inter-diffusion at elevated temperatures.

Stoichiometric CrN was evaluated as a diffusion barrier for metallic Cr coatings [48]. A thin CrN layer was ineffective at elevated temperatures because of a phase transformation (from CrN to Cr_2N + N_2 induced by inward diffusion of N) and concomitant cracking. A thick CrN layer (13 μm) demonstrated satisfactory performance, which prohibited Cr-diffusion into the substrate and Cr-Zr melting above 1350°C during exposure in steam for a short period (2 min). Additionally, inward diffusion of nitrogen resulted in formation of a thin stable ZrN layer at the coating/substrate interface.

A thin TiC interlayer has been proposed as a diffusion barrier between Ti_2AlC coatings and Zr alloy substrates [120]. The TiC barrier can suppress the rapid inward diffusion of Al into the substrate at 800°C; however, the coating system failed at elevated temperatures in steam owing to their low oxidation resistance.

Both Mo [28,50,64,154] and ZrO_2 [82] have been examined as a buffer layer for FeCrAl coatings. Negligible inter-diffusion between the coating and substrate was seen during oxidation to 1200°C. **Figure 22** compares the oxidation performance of coatings with and without a diffusion barrier. The oxidation rate of a single-layer FeCrAl coated specimen was even faster than an uncoated one at 1000°C in steam owing to Fe-Zr eutectic reaction, **Figure 22** (a). Significantly reduced oxidation kinetics was observed after applying a ZrO_2 buffer layer synthesized by plasma

electrolytic oxidation [82]. As seen in **Figure 22** (b), the alloying elements in the cold-sprayed FeCrAl coating penetrated the whole cladding tube tested in air at 1200°C for 20 min. Under identical conditions, a Mo buffer layer with around 20 μm thickness successfully suppressed the inter-diffusion between the FeCrAl coating and Zr alloy substrate [50]. The eutectic reaction temperatures of Zr-Mo and Fe-Mo [161] are at 1550°C and 1450°C, both considerably higher than that of Zr-Fe (~930°C, **Figure 17)**.

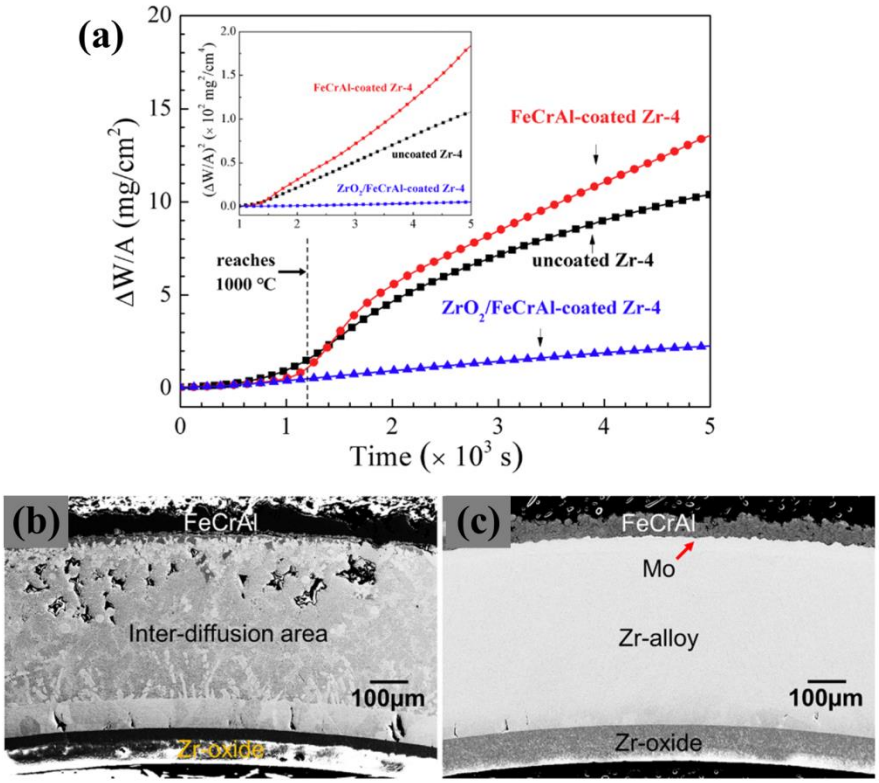

Figure 22 *Comparison of oxidation rate and microstructure of FeCrAl coatings on Zr alloy substrate without and with diffusion barrier. (a) Oxidation rate at 1000°C in steam without or with ZrO_2 interlayer [82], cross-sectional images after oxidation at 1200°C in air for 20 min (b) without and (c) with Mo interlayer [50].*

5.2 Severe accidents

Only a few studies have been dedicated to understanding the protective effect and failure mechanisms of various coating-substrate systems under simulated severe accident scenarios. The available data are largely regarding Cr-based coatings (like metallic Cr, CrN and Cr_2AlC MAX phase). The principal degradation mechanisms, except oxidation failure, identified with respect to metallic coatings and ceramic coatings during severe accidents (beyond 1200°C) are the formation of a liquid phase via eutectic reaction and brittle cracking, respectively.

Metallic Cr coatings reveal the capability to prevent the Zr alloy substrates from rapid oxidation and oxygen ingress up to 1300°C in steam, depending on coating

thickness [54]. At temperatures above the Zr-Cr eutectic temperature (~1330°C), formation of liquid phase accompanied by its continuous displacement triggers rapid failure of the coated cladding. Accelerated Cr interaction with Zr alloy substrates drives the chromium into the inner regions of the cladding corresponding to the prior β-Zr phase owing to oxygen diffusion. Brachet et al. observed a fairly homogeneous and uniform ZrO_2 layer on the Cr coated cladding after being tested to 1450°C (100 s) in steam, even though the surface became convoluted with many protrusions and blisters. The authors suggested that formation of a liquid Zr-Cr phase might not drastically modify the oxidation mechanisms and kinetics of the Zr alloy cladding in high-temperature steam environment [43]. On the other hand, a slightly thicker ZrO_2 layer and higher oxidation rate of the Cr coated surface was also reported relative to the un-coated surface at 1400°C (2 min) in steam [48]. Transient oxidation of an cold-sprayed Cr coated cladding tubes up to 1500°C in steam resulted in accelerated hydrogen release rate once the temperature exceeded the Cr-Zr eutectic temperature. Subsequently, the hydrogen release rate increased steeply at temperatures above ~1450°C and surpassed that of the uncoated reference Zircaloy-4, indicating a considerably faster oxidation rate [52].

Krejci et al. have tested single-layer sub-stoichiometric $Cr_{90}N_{10}$ coatings and two bilayer coatings: thin CrN/Cr (3/19 µm) and thick CrN/Cr (13/25 µm) on Zr alloys in steam above the Cr-Zr eutectic temperature [48]. Failure of the single-layer $Cr_{90}N_{10}$ and the thin CrN/Cr coated surfaces with melting plus a thicker oxide layer was seen after testing at 1400°C in steam for 2 min. The thick CrN/Cr multilayer coatings survived at 1365°C in steam for 2 min without coating-substrate melting, coating spallation or local coating failures, as shown in **Figure 23**. A thin ZrN layer formed at the coating/substrate interface, preventing diffusion of chromium into the Zr alloy substrate. Oxygen penetrated the coating layer, forming an α-Zr(O) layer underneath the coatings. The oxidized specimen moreover demonstrated a high residual ductility during ring compression tests. These promising results motivated the authors to develop functional gradient coatings based on Cr and CrN for the ATF application.

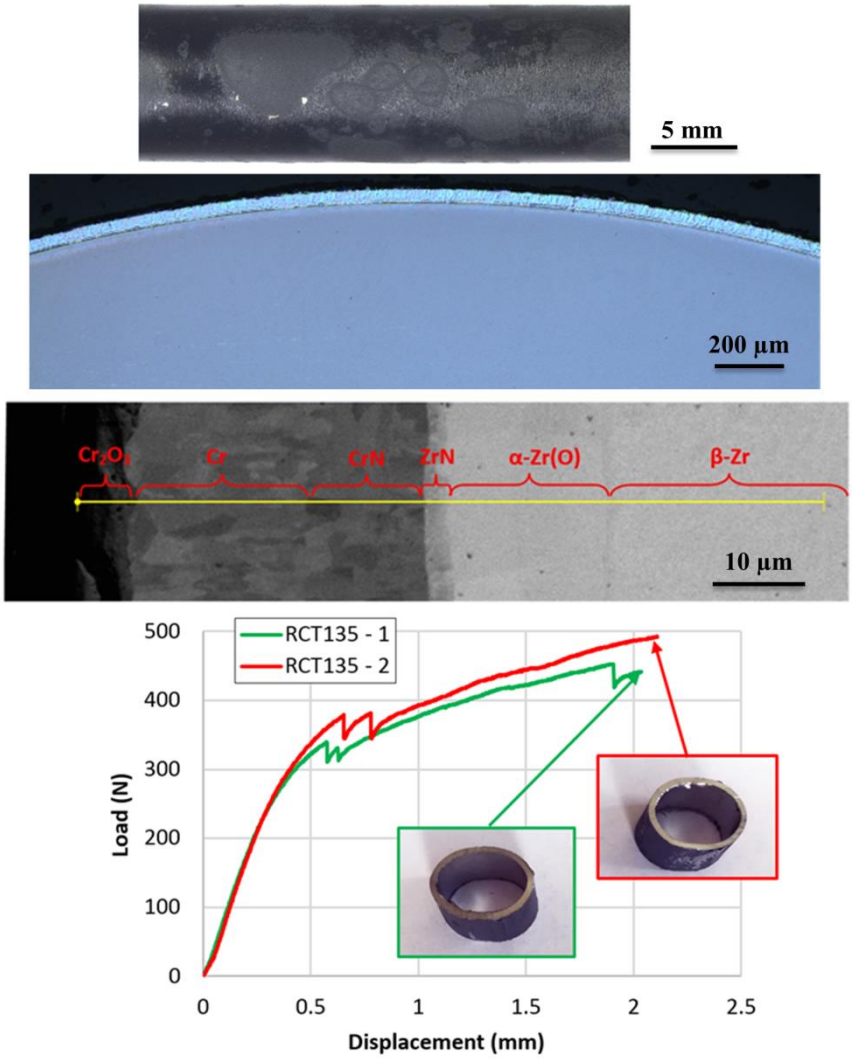

Figure 23 Appearance, microstructure and ring compression of thick CrN/Cr (13/25 µm) coated Zr alloy after oxidation at 1365°C for 2 min in steam.

Figure 24 compares the hydrogen release rate and the oxide layer thickness of thin Cr_2AlC coated (6 µm) and uncoated Zircaloy-4 from a transient oxidation test heating from 500°C to 1400°C in steam. As concluded from **Figure 24** (a) and (c), the coatings cracked at ~ 1260°C. After coating cracking the hydrogen release rate increased abruptly and the oxidation rate of the coated sample surpassed the uncoated one at around 1300°C. An inhomogeneous oxide layer was observed after testing, with a thicker layer beneath the cracks on the coated sample. However, there was no apparent evidence indicating liquid phase formation between the coating layer and the Zr alloy substrate after testing. Selective oxidation of Al in Cr_2AlC coatings typically leaves a Cr-C layer beneath, which probably increased the eutectic reaction temperature of the system [162].

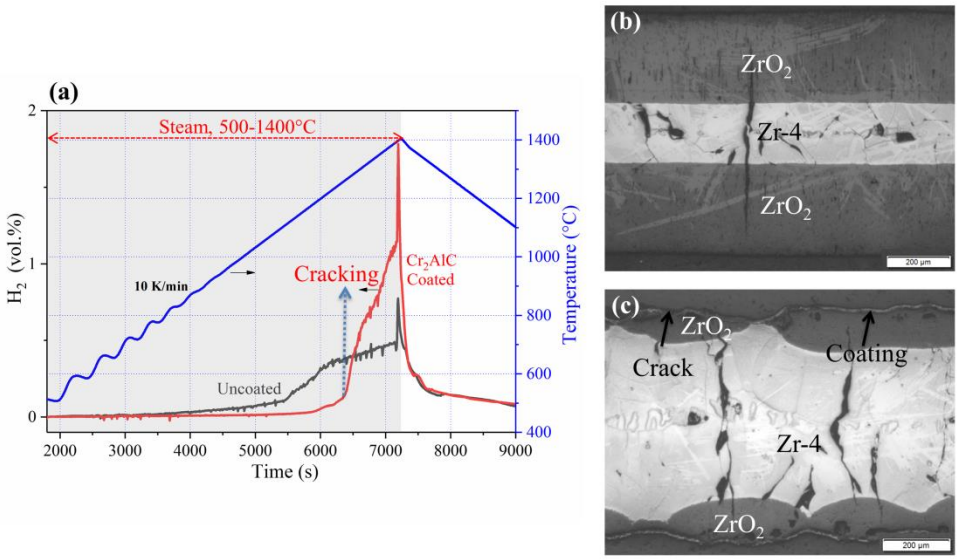

Figure 24 *(a)* Hydrogen release rate of a transient test from 500°C to 1400°C in steam and cross-sectional SEM images of (b) uncoated and (c) Cr_2AlC coated Zircaloy-4 after testing.

6. Conclusion and outlook

Surface modification of state-of-the-art zirconium-based alloy fuel claddings with innovative high-temperature oxidation/corrosion resistant metallic or ceramic coatings are being intensively pursued for enhanced accident tolerant fuel cladding applications. This approach represents a near-term evolutionary strategy and allows for an easier licensing pathway compared to alternative cladding materials.

A variety of materials have been proposed and examined and the principal coating concepts comprise metallic coatings, ceramic coatings and multilayer coatings. Multilayer coating designs are anticipated to overcome or alleviate the limitations of single-layer metallic (high interdiffusion rate and low eutectic reaction temperature with underlying Zr alloy substrate) and ceramic (low fracture toughness) coatings. Cr-based coatings (for instance pure Cr, CrN and Cr_2AlC) represent some of the most attractive and promising options considering their satisfactory performances under both normal and accident conditions.

The nature and performance of the coated claddings are highly affected by the constituent and microstructure of the coating-substrate system, which depends on the applied fabrication technology and concurrent processing parameters. Physical vapor deposition and cold spraying are the two prevalent coating methods for coated ATF application. The typically low deposition temperature and thin coating thickness via PVD processing are favored because of the negligible impact on microstructure modification of the substrate and neutronic economy. Thick coatings can be straightforwardly achieved via spraying processes. However, compositional, structural and mechanical inhomogeneities for sprayed coating-substrate systems have been frequently seen.

The specific application characteristics of enhanced ATF claddings require the coating materials to resist hydrothermal corrosion (normal operation) and high-temperature steam/air oxidation (accident scenarios). Both working environments require growth of a thermodynamically stable and protective oxide layer that acts as an effective diffusion barrier. The robust oxide scales that can endure at elevated temperatures in oxidizing atmosphere (accident scenarios) are those made of chromia, alumina or silica. The fast growth rate of Cr_2O_3 scale accompanied by formation of volatile hydroxides at elevated temperatures generally restricts its application to lower temperatures (ca. 1300°C). However, Al_2O_3 and SiO_2 are unstable via formation of soluble aqueous ions under normal operation conditions. Si- and Al-containing coatings often experience rapid hydrothermal dissolution or selective leaching of these two elements (or oxides) during autoclave testing.

The structural integrity of the coating-substrate system obviously will be highly challenged in the reactor core due to various stresses, irradiation damage and, during accident scenarios, by rapid degradation (like ballooning and burst) of the fuel cladding substrate. Ideally, the coating should be highly adherent under a variety of working conditions or self-healing after defects have occurred. Pure Cr coated claddings display satisfactory performances under out-of-pile irradiation testing and one cycle in-pile testing. Ceramic coatings are vulnerable to cracking and spallation owing to their brittle characteristics and low toughness. During design-basis and/or severe accident conditions, the principal degradation mechanisms, except oxidation failure, identified with respect to metallic coatings and ceramic coatings are the formation of liquid phases via eutectic reaction and brittle cracking, respectively.

Numerous coating concepts have been proposed as enhanced ATF claddings and the majority of studies to date mainly focus on testing and verifying their feasibility under out-of-pile conditions in case of hydrothermal corrosion and/or high-temperature oxidation. A comprehensive assessment and qualification of the coating-substrate system under long-term in-pile and (severe) accident conditions are required. Many knowledge gaps still exist, for instance the irradiation performance especially the chemical and physical stability of interfaces, mechanical behavior and degradation mechanisms under various situations. In addition, standard test methods and new failure criteria are needed to allow various coating concepts to be easily assessed and their applicability validated.

Acknowledgments

The authors acknowledge the HGF programs NUSAFE and STN at Karlsruhe Institute of Technology. Special thanks to Prof. Elizabeth J. Opila for reviewing the language.

References

1. Karoutas, Z.; Brown, J.; Atwood, A.; et al. *Progress in Nuclear Energy* **2018,** *102*: 68–78.
2. Terrani, K. A.; Zinkle, S. J.; Snead, L. L. *Journal of Nuclear Materials* **2014,** *448*: 420–435.
3. Motta, A. T.; Couet, A.; Comstock, R. J. *Annual Review of Materials Research* **2015,** *45*: 311–343.
4. Zinkle, S. J.; Terrani, K. A.; Gehin, J. C.; et al. *Journal of Nuclear Materials* **2014,** *448*: 374–379.
5. Steinbrück, M.; Vêr, N.; Große, M. *Oxidation of Metals* **2011,** *76*: 215–232.
6. Motta, A. T.; Capolungo, L.; Chen, L.-Q.; et al. *Journal of Nuclear Materials* **2014,** *448*: 374–379.
7. Terrani, K. A. *Journal of Nuclear Materials* **2018,** *501*: 13–30.
8. Bragg-Sitton, S. *Nuclear News* **2014,** *53*: 83–91.
9. Duan, Z.; Yang, H.; Satoh, Y.; et al. *Nuclear Engineering and Design* **2017,** *316*: 131–150.
10. Tang, C.; Stueber, M.; Seifert, H. J.; Steinbrueck, M. *Corrosion Reviews* **2017,** *35*: 141–166.
11. NEA No. 7317. *State-of-the-Art Report on Light Water Reactor Accident-Tolerant Fuels*, 2018.
12. Dryepondt, S.; Unocic, K. A.; Hoelzer, D. T.; et al. *Journal of Nuclear Materials* **2018,** *501*: 59–71.
13. Cheng, B.; Kim, Y. J.; Chou, P. *Nuclear Engineering and Technology* **2016,** *48*: 16–25.
14. Ben-Belgacem, M.; Richet, V.; Terrani, K. A.; et al. *Journal of Nuclear Materials* **2014,** *447*: 125–142.
15. Lomello, F.; Maskrot, H.; Meillot, E.; et al. *Comptes Rendus Physique* **2018,** *19*: 755–768.
16. Zinkle, S. J.; Was, G. S. *Acta Materialia* **2013,** *61*: 735–758.
17. Baney, R. H.; Tulenko, J. S. *An Innovative Ceramic Corrosion Protection System for Zircaloy Cladding*, 2003.
18. Wiklund, U.; Hedenqvist, P.; Hogmark, S.; et al. *Surface and Coatings Technology* **1996,** *86–87*: 530–534.
19. Sung, J. H.; Kim, T. H.; Kim, S. S. *Wear* **2001,** *250*: 658–664.
20. Michau, A.; Maury, F.; Schuster, F.; et al. *Inner-Side Coatings for Advanced Fuel Claddings Processed by DLI-MOCVD*. In *2017 Water Reactor Fuel Performance Meeting*; Jeju Island, Korea, 2017, pp 1–8.
21. Michau, A.; Maury, F.; Schuster, F.; et al. *Surface and Coatings Technology* **2018,** *349*: 1048–1057.
22. Azevedo, C. R. F. *Engineering Failure Analysis* **2011,** *18*: 1943–1962.
23. Idarraga-Trujillo, I.; Flem, M. L. E.; Brachet, J.-C.; et al. *Assessment At Cea of Coated Nuclear Fuel Cladding for LWRs With Increased Margins in LOCA and Beyond LOCA Conditions*. In *TopFuel 2013*; Charlotte, USA, 2013, pp 860–867.
24. Kam, D. H.; Lee, J. H.; Lee, T.; Jeong, Y. H. *Annals of Nuclear Energy* **2015,** *76*: 335–342.
25. Park, J.-H.; Kim, H.-G.; Park, J.; et al. *Surface and Coatings Technology* **2015,** *280*: 256–259.
26. Kim, H.-G.; Kim, I.-H.; Jung, Y.-I.; et al. *Journal of Nuclear Materials* **2015,** *465*: 531–539.
27. Brachet, J. C.; Saux, M. Le; Flem, M. Le; et al. *On-Going Studies at CEA on Chromium Coated Zirconium Based Nuclear Fuel Claddings for Enhanced Accident Tolerant LWRs Fuel*. In *TopFuel 2015*; Zurich, Switzerland, 2015, pp 31–38.
28. Park, D. J.; Kim, H. G.; Jung, Y. Il; et al. *Journal of Nuclear Materials* **2016,** *482*: 75–82.

29. Bischoff, J.; Vauglin, C.; Delafoy, C.; et al. *Development of Cr-Coated Zirconium Alloy Cladding for Enhanced Accident Tolerance*. In *TopFuel 2016*; Boise, USA, 2016, pp 1165–1171.
30. Brachet, J. C.; Le Saux, M.; Lezaud-Chaillioux, V.; et al. *Behavior under LOCA Conditions of Enhanced Accident Tolerant Chromium Coated Zircaloy-4 Claddings*. In *TopFuel 2016*; Boise, USA, 2016, pp 1173–1178.
31. Brachet, J. C.; Dumerval, M.; Lezaud-Chaillioux, V.; et al. *Behavior of Chromium Coated M5 Claddings under LOCA Conditions.* In *2017 Water Reactor Fuel Performance Meeting*; Jeju Island, Korea, 2017, pp 1–11.
32. Shah, H.; Romero, J.; Xu, P.; et al. *Development of Surface Coatings for Enhanced Accident Tolerant Fuel.* In 2017 *Water Reactor Fuel Performance Meeting*; Jeju Island, Korea, 2017, pp 1–8.
33. Ribis, J.; Wu, A.; Brachet, J.-C.; et al. *Journal of Materials Science* **2018,** *53*: 9879–9895.
34. Wu, A.; Ribis, J.; Brachet, J. C.; et al. *Journal of Nuclear Materials* **2018,** *504*: 289–299.
35. Maier, B. R.; Yeom, H.; Johnson, G.; et al. *Journal of Nuclear Materials* **2018,** *512*: 320–323.
36. Seshadri, A.; Shirvan, K. *Nuclear Engineering and Design* **2018,** *338*: 5–15.
37. Yeom, H.; Dabney, T.; Johnson, G.; et al. *International Journal of Advanced Manufacturing Technology* **2018,** 1373–1382.
38. Kuprin, A. S.; Belous, V. A.; Voyevodin, V. N.; et al. *Journal of Nuclear Materials* **2018,** *510*: 163–167.
39. Zhong, W.; Mouche, P. A.; Heuser, B. J. *Journal of Nuclear Materials* **2018,** *498*: 137–148.
40. Wagih, M.; Spencer, B.; Hales, J.; Shirvan, K. *Annals of Nuclear Energy* **2018,** *120*: 304–318.
41. Ševeček, M.; Gurgen, A.; Seshadri, A.; et al. *Nuclear Engineering and Technology* **2018,** *50*: 229–236.
42. Brachet, J.; Guilbert, T.; Saux, M. Le; et al. *Behavior of Cr-Coated M5 Claddings during and after High Temperature Steam Oxidation from 800 °C up to 1500 °C*. In *TopFuel 2018*; Prague, Czech Republic, 2018, pp 1–11.
43. Dumerval, M.; Houmaire, Q.; Brachet, J. C.; et al. *Behavior of Chromium Coated M5 Claddings upon Thermal Ramp Tests under Internal Pressure (Loss-of-Coolant Accident Conditions)*. In *TopFuel 2018*; Prague, Czech Republic, 2018, pp 1–8.
44. Delafoy, C.; Bischoff, J. *Benefits of Framatome's E-ATF Evolutionary Solution: Cr-Coated Cladding with Cr_2O_3-Doped Fuel*. In *TopFuel 2018*; Prague, Czech Republic, 2018, pp 1–11.
45. Bischoff, J.; Delafoy, C.; Chaari, N.; et al. *Cr Coated Cladding Development At Framatome*. In *TopFuel 2018*; Prague, Czech Republic, 2018, pp 1–7.
46. Giradrin, G.; Meier, R.; Jatuff, F.; et al. *Inspection Capabilities and In-Pile Experience with Innovative and Enhanced Accident Tolerant Fuel Materials at KKG*. In *TopFuel 2018*; Prague, Czech Republic, 2018, pp 1–10.
47. Ševecek, M.; Krejci, J.; SHAHIN, M. H.; et al. *Fatigue Behavior of Cold Spray - Coated Accident Tolerant*. In *TopFuel 2018*; Prague, Czech Republic, 2018, pp 1–15.
48. Krejci, J.; Sevecek, M.; Kabativa, J.; et al. *Experimental Behavior of Chromium-Based Coatings*. In *TopFuel 2018*; Prague, Czech Republic, 2018, pp 1–14.
49. Wang, Y.; Zhou, W.; Wen, Q.; et al. *Surface and Coatings Technology* **2018,** *344*: 141–148.
50. Maier, B.; Yeom, H.; Johnson, G.; et al. *Jom* **2018,** *70*: 198–202.
51. Bischoff, J.; Delafoy, C.; Vauglin, C.; et al. *Nuclear Engineering and Technology* **2018,** *50*: 223–228.
52. Tang, C.; Steinbrueck, M.; Grosse, M. *Oxidation Performance and Failure Behavior of Monolithic and Coated ATF Claddings under Severe Accident Conditions.* In *Technical Meeting*

on Modelling of Fuel Behaviour in Design Basis Accidents and Design Extension Conditions; Shenzhen, China, 2019, pp 1–8.
53. Brachet, J.-C.; Idarraga-Trujillo, I.; Flem, M. Le; et al. *Journal of Nuclear Materials* **2019,** *517*: 268–285.
54. Maier, B.; Yeom, H.; Johnson, G.; et al. *Journal of Nuclear Materials* **2019,** *519*: 247–254.
55. He, X.; Tian, Z.; Shi, B.; et al. *Annals of Nuclear Energy* **2019,** *132*: 243–248.
56. Han, X.; Xue, J.; Peng, S.; Zhang, H. *Corrosion Science* **2019,** *156*: 117–124.
57. Zhang, W.; Tang, R.; Yang, Z. B.; et al. Preparation, *Surface and Coatings Technology* **2018,** *347*: 13–19.
58. Zhang, Y.; Zuo, T. T.; Tang, Z.; et al. *Progress in Materials Science* **2014,** *61*: 1–93.
59. Barsoum, M. W. *Progress in Solid State Chemistry* **2000,** *28*: 201–281.
60. Eklund, P.; Beckers, M.; Jansson, U.; et al. *Thin Solid Films* **2010,** *518*: 1851–1878.
61. Zinkle, S. J.; Kinoshita, C. *Journal of Nuclear Materials* **1997,** *251*: 200–217.
62. Alat, E.; Motta, A. T.; Comstock, R. J.; et al. *Surface and Coatings Technology* **2015,** *281*: 133–143.
63. He, H.; Zhu, W.; Zhu, H.; et al. *Materials Research Express* **2018,** *6*: 026420.
64. Yeom, H.; Maier, B.; Johnson, G.; et al. *Journal of Nuclear Materials* **2018,** *507*: 306–315.
65. Alat, E.; Motta, A. T.; Comstock, R. J.; et al. *Journal of Nuclear Materials* **2016,** *478*: 236–244.
66. Alat, E.; Brova, M. J.; Younker, I. M.; et al. *Journal of Nuclear Materials* **2019,** .
67. Stueber, M.; Holleck, H.; Leiste, H.; et al. *Journal of Alloys and Compounds* **2009,** *483*: 321–333.
68. Wieciński, P.; Smolik, J.; Garbacz, H.; Kurzydłowski, K. J. *Surface and Coatings Technology* **2014,** *240*: 23–31.
69. Ding, X. Z.; Chen, G.; Amin-Ahmadi, B.; et al. *Thin Solid Films* **2015,** *578*: 133–138.
70. Petrov, I.; Barna, P. B.; Hultman, L.; Greene, J. E. *Journal of Vacuum Science & Technology A: Vacuum, Surfaces, and Films* **2003,** *21*: S117.
71. Younker, I.; Fratoni, M. *Progress in Nuclear Energy* **2016,** *88*: 10–18.
72. Fejt, F.; Sevecek, M.; Frybort, J.; Novak, O. *Annals of Nuclear Energy* **2019,** *124*: 579–591.
73. Assadi, H.; Kreye, H.; Gärtner, F.; Klassen, T. *Acta Materialia* **2016,** *116*: 382–407.
74. Park, D. J.; Kim, H. G.; Jung, Y. Il; et al. *Journal of Nuclear Materials* **2018,** *504*: 261–266.
75. Tang, C.; Grosse, M. K.; Trtik, P.; et al. *Acta Polytechnica* **2018,** *58*: 69–76.
76. Maier, B. R.; Garcia-Diaz, B. L.; Hauch, B.; et al. *Journal of Nuclear Materials* **2015,** *466*: 712–717.
77. Kaushal, A.; Prakash, J.; Dasgupta, K.; Chakravartty, J. K. *Nuclear Engineering and Design* **2016,** *303*: 122–131.
78. Al-Olayyan, Y.; Fuchs, G. E.; Baney, R.; Tulenko, J. *Journal of Nuclear Materials* **2005,** *346*: 109–119.
79. Škarohlíd, J.; Ashcheulov, P.; Škoda, R.; et al. *Scientific Reports* **2017,** *7*: 6469.
80. Ashcheulov, P.; Škoda, R.; Škarohlíd, J.; et al. *Applied Surface Science* **2015,** *359*: 621–628.
81. Kim, J.-M.; Ha, T.-H.; Kim, I.-H.; Kim, H.-G. *Metals* **2017,** *7*: 59.
82. Liu, K.; Li, Y.; Wang, J.; Ma, Q. *Journal of Alloys and Compounds* **2015,** *624*: 234–240.
83. Luscher, W. G.; Gilbert, E. R.; Pitman, S. G.; Love, E. F. *Journal of Nuclear Materials* **2013,** *433*: 514–522.
84. Wang, Y.; Tang, H.; Han, X.; et al. *Surface and Coatings Technology* **2018,** *349*: 807–815.
85. Lee, C. M.; Sohn, D. S. *Corrosion Science* **2018,** *131*: 116–125.

86. Kim, H.; Kim, I.; Jung, Y.; et al. *Nuclear Engineering and Technology* **2014,** *46*: 521–528.
87. Kim, H. G.; Kim, I. H.; Jung, Y. Il; et al. *Journal of Nuclear Materials* **2018,** *510*: 93–99.
88. Dong, Y.; Zhu, H.; Ge, F.; et al. *Surface and Coatings Technology* **2019,** *374*: 393–401.
89. Tang, C. Synthesis and High-Temperature Oxidation of Ternary Carbide Coatings on Zirconium-Based Alloy Cladding, Karlsurhe Institute of Technology, 2019.
90. Kritzer, P.; Boukis, N.; Dinjus, E. *Journal of Supercritical Fluids* **1999,** *15*: 205–227.
91. Cook, W. G.; Olive, R. P. *Corrosion Science* **2012,** *55*: 326–331.
92. Cook, W. G.; Olive, R. P. *Corrosion Science* **2012,** *58*: 291–298.
93. Cook, W. G.; Olive, R. P. *Corrosion Science* **2012,** *58*: 284–290.
94. Park, S. T. Amorphous Alumina Oxidation Protective Coating for Zircaloy Based on a Compositional Gradient Layer Systerm, University of Florida, 2004.
95. Zhao, X.; Guo, Y.; Guo, F.; et al. *Journal of Nuclear Materials* **2018,** *508*: 411–422.
96. Besmann, T. M.; Kulkarni, N. S.; Spear, K. E. *Journal of the American Ceramic Society* **2006,** *89*: 638–644.
97. Park, D.; Mouche, P. A.; Zhong, W.; et al. *Journal of Nuclear Materials* **2018,** *502*: 95–105.
98. Zhong, W.; Mouche, P. A.; Han, X.; et al. *Journal of Nuclear Materials* **2016,** *470*: 327–338.
99. Terrani, K. A.; Pint, B. A.; Kim, Y. J.; et al. *Journal of Nuclear Materials* **2016,** *479*: 36–47.
100. Yeom, H.; Lockhart, C.; Mariani, R.; et al. *Journal of Nuclear Materials* **2018,** *499*: 256–267.
101. Waliś, L.; Rydzewski, M.; Semina, V. K.; et al. *Nukleonika* **2018,** *63*: 73–79.
102. Yeom, H.; Maier, B.; Mariani, R.; et al. *Surface and Coatings Technology* **2017,** *316*: 30–38.
103. Cheol Lee, G.; Noh, H.; Yeom, H.; et al. *Annals of Nuclear Energy* **2019,** *126*: 350–358.
104. Kim, J.; Kim, H. G.; Ryu, H. J. High Temperature Oxidation Behavior of $ZrSi_2$ and Its Coating on the Surface of Zircaloy-4 Tube by 3D Laser Coating Method. In *Transactions of the Korean Nuclear Society Spring Meeting*; Jeju Island, Korea, 2018, pp 1–4.
105. Son, G. M.; Kim, K. M.; Bang, I. C. *International Journal of Heat and Mass Transfer* **2018,** *118*: 890–899.
106. Bao, W.; Xue, J.; Liu, J. X.; et al. *Journal of Alloys and Compounds* **2018,** *730*: 81–87.
107. Lee, K.; Kim, D.; Yoon, Y. S. *Thin Solid Films* **2018,** *660*: 221–230.
108. Ren, D.; Wang, J.; Eklund, P.; et al. *Vacuum* **2018,** *160*: 128–132.
109. Tang, C.; Stueber, M.; Steinbrueck, M.; et al. *Evaluation of Magnetron Sputtered Protective Zr-Al-C Coatings for Accident Tolerant Zircaloy Claddings*. In *2017 Water Reactor Fuel Performance Meeting*; Jeju Island, Korea, 2017, pp 1–9.
110. Khatkhatay, F.; Jiao, L.; Jian, J.; et al. *Journal of Nuclear Materials* **2014,** *451*: 346–351.
111. Kuprin, A. S.; Belous, V. A.; Voyevodin, V. N.; et al. *Journal of Nuclear Materials* **2015,** *465*: 400–406.
112. Sagás, J. C.; Edmondson, P. D.; Donnelly, S. E.; et al. *Journal of Nuclear Materials* **2018,** *512*: 239–245.
113. Ren, Y.; Zou, S.; Lei, M.; et al. *Journal of Nuclear Materials* **2018,** *509*: 542–549.
114. Wu, Y.; Ma, X.; Meng, C.; et al. *Journal of Nuclear Materials* **2019,** *515*: 354–369.
115. Liu, Y.; Bhamji, I.; Withers, P. J.; et al. *Journal of Nuclear Materials* **2015,** *466*: 718–727.
116. Pauley, M. A.; Motta, A. T.; Alat, E.; et al. *Surface and Coatings Technology* **2017,** *331*: 163–171.
117. Daub, K.; Nieuwenhove, R. Van; Nordin, H. *Journal of Nuclear Materials* **2015,** *467*: 260–270.
118. Yeom, H.; Hauch, B.; Cao, G.; et al. *Thin Solid Films* **2016,** *615*: 202–209.

119. Wang, J.; Shu, R.; Dong, Y.; et al. *Scripta Materialia* **2017,** *137*: 13–17.
120. Tang, C.; Steinbrueck, M.; Stueber, M.; et al. *Corrosion Science* **2018,** *135*: 87–98.
121. Zhang, J.; Tian, Z.; Zhang, H.; et al. *Journal of Materials Science & Technology* **2019,** *35*: 1–5.
122. Tallman, D. J.; Anasori, B.; Barsoum, M. W. *Materials Research Letters* **2013,** *1*: 115–125.
123. Tang, C.; Steinbrueck, M.; Grosse, M.; et al. *Improvement of the High-Temperature Oxidation Resistance of Zr Alloy Cladding by Surface Modification with Aluminum-Containing Ternary Carbide Coatings*. In *International Congress on Advances in Nuclear Power Plants*; Charlotte, USA, 2018, pp 694–700.
124. Ward, J.; Bowden, D.; Prestat, E.; et al. *Corrosion Science* **2018,** *139*: 444–453.
125. Ivanova, S. V.; Glagovsky, E. M.; Nikonorov, K. Y.; et al. *Methods to Increase Corrosion Stability and Wear Resistance of LWR Active Core Zirconium Components during Operation and in Conditions of Loss-of-Coolant Accident*. In *TopFuel 2013*; Charlotte, USA, 2013, pp 334–350.
126. Zhang, W.; Tang, R.; Yang, Z. B.; et al. *Journal of Nuclear Materials* **2018,** *512*: 15–24.
127. Zhang, W.; Wang, M.; Wang, L.; et al. *Applied Surface Science* **2019,** *485*: 108–118.
128. Lee, Y.; Lee, J. I.; No, H. C. *Nuclear Engineering and Technology* **2017,** *49*: 1031-1043.
129. Lee, Y. H.; Park, J. H.; Kim, I. H.; et al. *Journal of Nuclear Materials* **2019,** *523*: 223–230.
130. Capps, N.; Mai, A.; Kennard, M.; Liu, W. *Nuclear Engineering and Design* **2018,** *332*: 383–391.
131. Zinkle, S. J.; Busby, J. T. *Materials Today* **2009,** *12*: 12–19.
132. Kratochvílová, I.; Skoda, R.; Skarohlíd, J.; et al. *Journal of Materials Processing Technology* **2014,** *214*: 2600–2605.
133. Bugnet, M.; Mauchamp, V.; Oliviero, E.; et al. *Journal of Nuclear Materials* **2013,** *441*: 133–137.
134. Gigax, J. G.; Kennas, M.; Kim, H.; et al. *Journal of Nuclear Materials* ***2019,*** *523: 26–32.*
135. Field, K. G.; Briggs, S. A.; Sridharan, K.; et al. *Journal of Nuclear Materials* **2017,** *489*: 118–128.
136. Sridharan, K.; Briggs, S. A.; Terrani, K. A.; et al. *Scripta Materialia* **2016,** *116*: 112–116.
137. Xiao, J.; Yang, T.; Wang, C.; et al. *Journal of the American Ceramic Society* **2015,** *98*: 1323–1331.
138. Tallman, D. J.; Hoffman, E. N.; Caspi, E. N.; et al. *Acta Materialia* **2015,** *85*: 132–143.
139. Wang, C.; Yang, T.; Tracy, C. L.; et al. *Acta Materialia* **2018,** *144*: 432–446.
140. Ang, C.; Silva, C.; Shih, C.; et al. *Scripta Materialia* **2016,** *114*: 74–78.
141. Shen, H. H.; Ao, L.; Li, F. Z.; et al. *Journal of Nuclear Materials* **2017,** *485*: 262–272.
142. Shah, H.; Romero, J.; Xu, P.; et al. *Westinghouse-Exelon EnCore ® Fuel Lead Test Rod (LTR) Program Including Coated Cladding Development and Advanced Pellets*. In *TopFuel 2018*; Prague, Czech Republic, 2018, pp 1–9.
143. Nieuwenhove, R. Van; Andersson, V.; Balak, J.; Oberländer, B. *In-Pile Testing of CrN, TiAlN and AlCrN Coatings on Zircaloy Cladding in the Halden Reactor*. In *18th International Symposium on Zirconium in the Nuclear Industry*; West Conshohocken, USA, 2018, pp 965–982.
144. Lee, K.-G.; In, W.-K.; Kim, H.-G. *Nuclear Engineering and Design* **2019,** *347*: 10–19.
145. Seshadri, A.; Phillips, B.; Shirvan, K. *International Journal of Heat and Mass Transfer* **2018,** *127*: 1087–1095.
146. Meschter, P. J.; Opila, E. J.; Jacobson, N. S. *Annual Review of Materials Research* **2013,** *43*: 559–588.
147. Young, D. J. *High Temperature Oxidation and Corrosion of Metals*. (2rd edn.). Elsevier: Netherlands, 2016.

148. Carr, J.; Vasudevamurthy, G.; Snead, L.; et al. *Journal of Materials Engineering and Performance* **2016,** *25*: 2347–2355.
149. Lukas, H.; Fries, S. G.; Sundman, B. *Computational Thermodynamics: The Calphad Method*. Cambridge university press, UK, 2007.
150. Kim, H.-G.; Kim, I.-H.; Park, J.-Y.; Koo, Y.-H. *Application of Coating Technology on Zirconium-Based Alloy to Decrease High-Temperature Oxidation.* In 18th International Symposium on Zirconium in the Nuclear Industry; West Conshohocken, USA, 2016, pp 346–369.
151. Dong, Y.; Ge, F.; Meng, F.; et al. *Surface and Coatings Technology* **2018,** *350*: 841–847.
152. Terrani, K. A.; Parish, C. M.; Shin, D.; Pint, B. A. *Journal of Nuclear Materials* **2013,** *438*: 64–71.
153. Gigax, J. G.; Kennas, M.; Kim, H.; et al. *Journal of Nuclear Materials* **2019,** *519*: 57–63.
154. Han, X.; Wang, Y.; Peng, S.; Zhang, H. *Corrosion Science* **2019,** *149*: 45–53.
155. Westwood, M. E.; Webster, J. D.; Day, R. J.; et al. *Journal of Materials Science* **1996,** *31*: 1389–1397.
156. Mayrhofer, P. H.; Rachbauer, R.; Holec, D.; et al. *Protective Transition Metal Nitride Coatings*; In *Comprehensive Materials Proceedings*. Elsevier: Netherlands, 2014, pp 355-388.
157. Qi, Z. B.; Wu, Z. T.; Wang, Z. C. *Surface and Coatings Technology* **2014,** *259*: 146–151.
158. Skarohlid, J.; Skoda, R. *High Temperature Behaviour of CrAlSiN MAX Phase Coatings on Zirconium Alloy*. In *2017 Water Reactor Fuel Performance Meeting*; Jeju Island, Korea, 2017, pp 1–5.
159. Ma, X. F.; Wu, Y. W.; Tan, J.; et al. *Surface and Coatings Technology* **2019,** *358*: 521–530.
160. Li, S.; Song, G.; Kwakernaak, K.; et al. *Journal of the European Ceramic Society* **2012,** *32*: 1813–1820.
161. OuYang, X.; Yin, F.; Hu, J.; et al. *Calphad: Computer Coupling of Phase Diagrams and Thermochemistry* **2018,** *63*: 212–219.
162. Hajas, D. E.; to Baben, M.; Hallstedt, B.; et al. *Surface and Coatings Technology* **2011,** *206*: 591–598.

Reference

1. Karoutas, Z. *et al.* The maturing of nuclear fuel: Past to Accident Tolerant Fuel. *Prog. Nucl. Energy* **102**, 68–78 (2018).

2. Terrani, K. A., Zinkle, S. J. & Snead, L. L. Advanced oxidation-resistant iron-based alloys for LWR fuel cladding. *J. Nucl. Mater.* **448**, 420–435 (2014).

3. Motta, A. T., Couet, A. & Comstock, R. J. Corrosion of zirconium alloys used for nuclear fuel cladding. *Annu. Rev. Mater. Res.* **45**, 311–343 (2015).

4. Zinkle, S. J., Terrani, K. A., Gehin, J. C., Ott, L. J. & Snead, L. L. Accident tolerant fuels for LWRs: A perspective. *J. Nucl. Mater.* **448**, 374–379 (2014).

5. Steinbrück, M., Vér, N. & Große, M. Oxidation of advanced zirconium cladding alloys in steam at temperatures in the range of 600-1200 °C. *Oxid. Met.* **76**, 215–232 (2011).

6. Motta, A. T. *et al.* Hydrogen in zirconium alloys: A review. *J. Nucl. Mater.* **518**, 440–460 (2019).

7. Terrani, K. A. Accident tolerant fuel cladding development: Promise, status, and challenges. *J. Nucl. Mater.* **501**, 13–30 (2018).

8. Bragg-Sitton, S. Development of advanced accident-tolerant fuels for commercial LWRs. *Nucl. News* **53**, 83–91 (2014).

9. Duan, Z. *et al.* Current status of materials development of nuclear fuel cladding tubes for light water reactors. *Nucl. Eng. Des.* **316**, 131–150 (2017).

10. Tang, C., Stueber, M., Seifert, H. J. & Steinbrueck, M. Protective coatings on zirconium-based alloys as accident-tolerant fuel (ATF) claddings. *Corros. Rev.* **35**, 141–166 (2017).

11. OECD-NEA. *State-of-the-Art Report on Light Water Reactor Accident-Tolerant Fuels*. (2018).

12. Dryepondt, S., Unocic, K. A., Hoelzer, D. T., Massey, C. P. & Pint, B. A. Development of low-Cr ODS FeCrAl alloys for accident-tolerant fuel cladding. *J. Nucl. Mater.* **501**, 59–71 (2018).

13. Cheng, B., Kim, Y. J. & Chou, P. Improving Accident Tolerance of Nuclear Fuel with Coated Mo-alloy Cladding. *Nucl. Eng. Technol.* **48**, 16–25 (2016).

14. Ben-Belgacem, M., Richet, V., Terrani, K. A., Katoh, Y. & Snead, L. L. Thermo-mechanical analysis of LWR SiC/SiC composite cladding. *J. Nucl. Mater.* **447**, 125–142 (2014).

15. Lomello, F. *et al.* Emerging processes for metallurgical coatings and thin films. *Comptes Rendus Phys.* **19**, 755–768 (2018).

16. Zinkle, S. J. & Was, G. S. Materials challenges in nuclear energy. *Acta Mater.* **61**, 735–758 (2013).

17. Baney, R. H. & Tulenko, J. S. *An Innovative Ceramic Corrosion Protection System for Zircaloy Cladding*. (2003).

18. Wiklund, U., Hedenqvist, P., Hogmark, S., Stridh, B. & Arbell, M. Multilayer coatings as corrosion protection of Zircaloy. *Surf. Coatings Technol.* **86–87**, 530–534 (1996).

19. Sung, J. H., Kim, T. H. & Kim, S. S. Fretting damage of TiN coated zircaloy-4 tube. *Wear* **250**, 658–664 (2001).

20. Michau, A. *et al.* Inner-Side Coatings for Advanced Fuel Claddings Processed by DLI-MOCVD. in *Water Reactor Fuel Performance Meeting* (2017).

21. Michau, A. *et al.* High-temperature oxidation resistance of chromium-based coatings deposited by DLI-MOCVD for enhanced protection of the inner surface of long tubes. *Surf. Coatings Technol.* **349**, 1048–1057 (2018).

22. Azevedo, C. R. F. Selection of fuel cladding material for nuclear fission reactors. *Eng. Fail. Anal.* **18**, 1943–1962 (2011).

23. Idarraga-Trujillo, I. *et al.* Assessment At Cea of Coated Nuclear Fuel Cladding for LWRs With Increased Margins in LOCA and Beyond LOCA Conditions. in *TopFuel 2013* 860–867 (2013).

24. Kam, D. H., Lee, J. H., Lee, T. & Jeong, Y. H. Critical heat flux for SiC- and Cr-coated plates under atmospheric condition. *Ann. Nucl. Energy* **76**, 335–342 (2015).

25. Park, J.-H. *et al.* High temperature steam-oxidation behavior of arc ion plated Cr coatings for accident tolerant fuel claddings. *Surf. Coatings Technol.* **280**, 256–259 (2015).

26. Kim, H.-G. *et al.* Adhesion property and high-temperature oxidation behavior of Cr-coated Zircaloy-4 cladding tube prepared by 3D laser coating. *J. Nucl. Mater.* **465**, 531–539 (2015).

27. Brachet, J. C. *et al.* On-going studies at CEA on chromium coated zirconium based nuclear fuel claddings for enhanced Accident Tolerant LWRs Fuel. in *TopFuel* 31–38 (2015).

28. Park, D. J. *et al.* Behavior of an improved Zr fuel cladding with oxidation resistant coating under loss-of-coolant accident conditions. *J. Nucl. Mater.* **482**, 75–82 (2016).

29. Bischoff, J. *et al.* Development of Cr-coated Zirconium Alloy Cladding for Enhanced Accident Tolerance. in *TopFuel* 1165–1171 (2016).

30. Brachet, J. C. *et al.* Behavior under LOCA conditions of Enhanced Accident Tolerant Chromium Coated Zircaloy-4 Claddings. in *TopFuel* 1173–1178 (2016).

31. Brachet, J. C. *et al.* Behavior of Chromium Coated M5 Claddings under LOCA Conditions. in *2017 Water Reactor Fuel Performance Meeting* 1–11 (2017).

32. Shah, H. *et al.* Development of Surface Coatings for Enhanced Accident Tolerant Fuel. in *Water Reactor Fuel Performance Meeting* (2017).

33. Ribis, J., Wu, A., Brachet, J.-C., Barcelo, F. & Arnal, B. Atomic-scale interface structure of a Cr-coated Zircaloy-4 material. *J. Mater. Sci.* **53**, 9879–9895 (2018).

34. Wu, A. *et al.* HRTEM and chemical study of an ion-irradiated chromium/zircaloy-4 interface. *J. Nucl. Mater.* **504**, 289–299 (2018).

35. Maier, B. R. *et al.* In situ TEM investigation of irradiation-induced defect formation in cold spray Cr coatings for accident tolerant fuel applications. *J. Nucl. Mater.* **512**, 320–323 (2018).

36. Seshadri, A. & Shirvan, K. Quenching heat transfer analysis of accident tolerant coated fuel cladding. *Nucl. Eng. Des.* **338**, 5–15 (2018).

37. Yeom, H. *et al.* Improving deposition efficiency in cold spraying chromium coatings by powder annealing. *Int. J. Adv. Manuf. Technol.* 1373–1382 (2018). doi:10.1007/s00170-018-2784-1

38. Kuprin, A. S. *et al.* Irradiation resistance of vacuum arc chromium coatings for zirconium alloy fuel claddings. *J. Nucl. Mater.* **510**, 163–167 (2018).

39. Zhong, W., Mouche, P. A. & Heuser, B. J. Response of Cr and Cr-Al coatings on Zircaloy-2 to high temperature steam. *J. Nucl. Mater.* **498**, 137–148 (2018).

40. Wagih, M., Spencer, B., Hales, J. & Shirvan, K. Fuel performance of chromium-coated zirconium alloy and silicon carbide accident tolerant fuel claddings. *Ann. Nucl. Energy* **120**, 304–318 (2018).

41. Ševeček, M. *et al.* Development of Cr cold spray–coated fuel cladding with enhanced accident tolerance. *Nucl. Eng. Technol.* **50**, 229–236 (2018).

42. Dumerval, M. *et al.* Behavior of chromium coated m5 claddings upon thermal ramp tests under internal pressure (loss-of-coolant accident conditions). in *TOPFUEL* 1–8 (2018).

43. Brachet, J. *et al.* Behavior of Cr-coated m5 claddings during and after high temperature steam oxidation from 800 °C up to 1500 °C. in *TopFuel* 1–11 (2018).

44. Delafoy, C. & Bischoff, J. Benefits of framatome's E-ATF evolutionary solution: Cr-coated cladding with Cr2O3-doped fuel. in *TOPFUEL* 1–11 (2018). doi:10.1155/2014/210146

45. Bischoff, J. *et al.* Cr coated cladding Development At Framatome. in *TOPFUEL* 1–7 (2018).

46. Giradin, G. *et al.* Inspection capabilities and in-pile experience with innovative and enhanced accident tolerant fuel materials at KKG. in *TOPFUEL* 1–10 (2018).

47. Ševecek, M. *et al.* Fatigue Behavior of Cold Spray - Coated Accident Tolerant. in *TOPFUEL* 1–15 (2018).

48. Krejci, J. *et al.* Experimental behavior of chromium-based coatings. in *TopFuel* 1–14 (2018).

49. Wang, Y. *et al.* Behavior of plasma sprayed Cr coatings and FeCrAl coatings on Zr fuel cladding under loss-of-coolant accident conditions. *Surf. Coatings Technol.* **344**, 141–148 (2018).

50. Maier, B. *et al.* Development of Cold Spray Coatings for Accident-Tolerant Fuel Cladding in Light Water Reactors. *Jom* **70**, 198–202 (2018).

51. Bischoff, J. *et al.* AREVA NP's enhanced accident-tolerant fuel developments: Focus on Cr-coated M5 cladding. *Nucl. Eng. Technol.* **50**, 223–228 (2018).

52. Tang, C., Steinbrueck, M. & Grosse, M. Oxidation performance and failure behavior of monolithic and coated ATF claddings under severe accident conditions. in *Technical Meeting on Modelling of Fuel Behaviour in Design Basis Accidents and Design Extension Conditions* 1–8 (2019).

53. Brachet, J.-C. *et al.* Early studies on Cr-Coated Zircaloy-4 as enhanced accident tolerant nuclear fuel claddings for light water reactors. *J. Nucl. Mater.* **517**, 268–285 (2019).

54. Maier, B. *et al.* Development of cold spray chromium coatings for improved accident tolerant zirconium-alloy cladding. *J. Nucl. Mater.* **519**, 247–254 (2019).

55. He, X. *et al.* Effect of gas pressure and bias potential on oxidation resistance of Cr coatings. *Ann. Nucl. Energy* **132**, 243–248 (2019).

56. Han, X., Xue, J., Peng, S. & Zhang, H. An Interesting Oxidation Phenomenon of Cr coatings on Zry-4 substrates in High Temperature Steam Environment. *Corros. Sci.* **156**, 117–124 (2019).

57. Zhang, W. *et al.* Preparation, structure, and properties of an AlCrMoNbZr high-

entropy alloy coating for accident-tolerant fuel cladding. *Surf. Coatings Technol.* **347**, 13–19 (2018).

58. Zhang, Y. *et al.* Microstructures and properties of high-entropy alloys. *Prog. Mater. Sci.* **61**, 1–93 (2014).

59. Barsoum, M. W. The MN+1AXN phases: a new class of solids; thermodynamically stable nanolaminates. *Prog. Solid State Chem.* **28**, 201–281 (2000).

60. Eklund, P., Beckers, M., Jansson, U., Högberg, H. & Hultman, L. The Mn+1AXn phases: Materials science and thin-film processing. *Thin Solid Films* **518**, 1851–1878 (2010).

61. Zinkle, S. J. & Kinoshita, C. Defect production in ceramics. *J. Nucl. Mater.* **251**, 200–217 (1997).

62. Alat, E., Motta, A. T., Comstock, R. J., Partezana, J. M. & Wolfe, D. E. Ceramic coating for corrosion (c3) resistance of nuclear fuel cladding. *Surf. Coatings Technol.* **281**, 133–143 (2015).

63. He, H. *et al.* Influence of the Cr interlayer on the microstructure of sputtered TiN coatings deposited on zirconium alloy. *Mater. Res. Express* **6**, 026420 (2018).

64. Yeom, H. *et al.* Development of Cold Spray Process for Oxidation-Resistant FeCrAlY and Mo Diffusion Barrier Coatings on Zr-alloy for Accident Tolerant Fuel Cladding in Light Water Reactors. *J. Nucl. Mater.* **507**, 306–315 (2018).

65. Alat, E., Motta, A. T., Comstock, R. J., Partezana, J. M. & Wolfe, D. E. Multilayer (TiN, TiAlN) ceramic coatings for nuclear fuel cladding. *J. Nucl. Mater.* **478**, 236–244 (2016).

66. Alat, E. *et al.* Neutronic and mechanical evaluation of rare earth doped and undoped nitride-based coatings for accident tolerant fuels. *J. Nucl. Mater.* **518**, 419–430 (2019).

67. Stueber, M. *et al.* Concepts for the design of advanced nanoscale PVD multilayer protective thin films. *J. Alloys Compd.* **483**, 321–333 (2009).

68. Wieciński, P., Smolik, J., Garbacz, H. & Kurzydłowski, K. J. Failure and deformation mechanisms during indentation in nanostructured Cr/CrN multilayer coatings. *Surf. Coatings Technol.* **240**, 23–31 (2014).

69. Ding, X. Z. *et al.* Thermal conductivity of titanium nitride/titanium aluminum nitride multilayer coatings deposited by lateral rotating cathode arc. *Thin Solid Films* **578**, 133–138 (2015).

70. Petrov, I., Barna, P. B., Hultman, L. & Greene, J. E. Microstructural evolution during film growth. *J. Vac. Sci. Technol. A Vacuum, Surfaces, Film.* **21**, S117 (2003).

71. Younker, I. & Fratoni, M. Neutronic evaluation of coating and cladding materials for accident tolerant fuels. *Prog. Nucl. Energy* **88**, 10–18 (2016).

72. Fejt, F., Sevecek, M., Frybort, J. & Novak, O. Study on neutronics of VVER-1200 with accident tolerant fuel cladding. *Ann. Nucl. Energy* **124**, 579–591 (2019).

73. Assadi, H., Kreye, H., Gärtner, F. & Klassen, T. Cold spraying – A materials perspective. *Acta Mater.* **116**, 382–407 (2016).

74. Park, D. J. *et al.* Microstructure and mechanical behavior of Zr substrates coated with FeCrAl and Mo by cold-spraying. *J. Nucl. Mater.* **504**, 261–266 (2018).

75. Kaushal, A., Prakash, J., Dasgupta, K. & Chakravartty, J. K. Simulation and experimental study of CVD process for low temperature nanocrystalline silicon carbide coating. *Nucl. Eng. Des.* **303**, 122–131 (2016).

76. Al-Olayyan, Y., Fuchs, G. E., Baney, R. & Tulenko, J. The effect of Zircaloy-4 substrate surface condition on the adhesion strength and corrosion of SiC coatings. *J. Nucl. Mater.* **346**, 109–119 (2005).

77. Škarohlíd, J. *et al.* Nanocrystalline diamond protects Zr cladding surface against oxygen and hydrogen uptake: Nuclear fuel durability enhancement. *Sci. Rep.* **7**, 6469 (2017).

78. Ashcheulov, P. *et al.* Thin polycrystalline diamond films protecting zirconium alloys surfaces: From technology to layer analysis and application in nuclear facilities. *Appl. Surf. Sci.* **359**, 621–628 (2015).

79. Kim, J.-M., Ha, T.-H., Kim, I.-H. & Kim, H.-G. Microstructure and Oxidation Behavior of CrAl Laser-Coated Zircaloy-4 Alloy. *Metals (Basel).* **7**, 59 (2017).

80. Liu, K., Li, Y., Wang, J. & Ma, Q. In-situ synthesized Ni – Zr intermetallic / ceramic reinforced composite coatings on zirconium substrate by high power diode laser. *J. Alloys Compd.* **624**, 234–240 (2015).

81. Luscher, W. G., Gilbert, E. R., Pitman, S. G. & Love, E. F. Surface modification of Zircaloy-4 substrates with nickel zirconium intermetallics. *J. Nucl. Mater.* **433**, 514–522 (2013).

82. Wang, Y. *et al.* Oxidation resistance improvement of Zr-4 alloy in 1000 °C steam environment using ZrO2/FeCrAl bilayer coating. *Surf. Coatings Technol.* **349**, 807–815 (2018).

83. Lee, C. M. & Sohn, D. S. Enhanced high-temperature oxidation resistance of a zirconium alloy cladding by high-temperature preformed oxide on the cladding. *Corros. Sci.* **131**, 116–125 (2018).

84. Kim, H. *et al.* Microstructure and Mechanical Strength of Surface ODS Treated Zircaloy-4 Sheet Using Laser Beam Scanning Laser. *Nucl. Eng. Technol.* **46**, 521–528 (2014).

85. Kim, H. G. *et al.* Out-of-pile performance of surface-modified Zr cladding for accident tolerant fuel in LWRs. *J. Nucl. Mater.* **510**, 93–99 (2018).

86. Dong, Y., Zhu, H., Ge, F., Zhao, G. & Huang, F. Microstructural effects on the high-temperature steam oxidation resistance of magnetron sputtered Cr-Al-Si-N quaternary coatings on zirconium coupons. *Surf. Coatings Technol.* **374**, 393–401 (2019).

87. Tang, C. Synthesis and high-temperature oxidation of ternary carbide coatings on zirconium-based alloy cladding. (2019).

88. Kritzer, P., Boukis, N. & Dinjus, E. Factors controlling corrosion in high-temperature aqueous solutions: A contribution to the dissociation and solubility data influencing corrosion processes. *J. Supercrit. Fluids* **15**, 205–227 (1999).

89. Cook, W. G. & Olive, R. P. Pourbaix diagrams for the iron--water system extended to high-subcritical and low-supercritical conditions. *Corros. Sci.* **55**, 326–331 (2012).

90. Cook, W. G. & Olive, R. P. Pourbaix diagrams for chromium, aluminum and titanium extended to high-subcritical and low-supercritical conditions. *Corros. Sci.* **58**, 291–298 (2012).

91. Cook, W. G. & Olive, R. P. Pourbaix diagrams for the nickel-water system extended to high-subcritical and low-supercritical conditions. *Corros. Sci.* **58**, 284–290 (2012).

92. Park, S. T. Amorphous alumina oxidation protective coating for zircaloy based on a compositional gradient layer systerm. (University of Florida, 2004).

93. Zhao, X. *et al.* Corrosion of the bonding at FeCrAl/Zr alloy interfaces in steam. *J. Nucl. Mater.* **508**, 411–422 (2018).

94. Besmann, T. M., Kulkarni, N. S. & Spear, K. E. Thermochemical Analysis and Modeling of the Al2O3–Cr2O3, Cr2O3–SiO2, and Al2O3–Cr2O3–SiO2 Systems Relevant to Refractories. *J. Am. Ceram. Soc.* **89**, 638–644 (2006).

95. Park, D. *et al.* TEM/STEM study of Zircaloy-2 with protective FeAl(Cr) layers under simulated BWR environment and high-temperature steam exposure. *J. Nucl. Mater.* **502**, 95–105 (2018).

96. Zhong, W. *et al.* Performance of iron-chromium-aluminum alloy surface coatings on Zircaloy 2 under high-temperature steam and normal BWR operating conditions. *J. Nucl. Mater.* **470**, 327–338 (2016).

97. Terrani, K. A. *et al.* Uniform corrosion of FeCrAl alloys in LWR coolant environments. *J. Nucl. Mater.* **479**, 36–47 (2016).

98. Yeom, H. *et al.* Evaluation of steam corrosion and water quenching behavior of zirconium-silicide coated LWR fuel claddings. *J. Nucl. Mater.* **499**, 256–267 (2018).

99. Waliś, L. *et al.* Studies on magnetron-sputtered zirconium-silicide coatings deposited on zirconium alloy for the enhancement of their high-temperature oxidation resistance. *Nukleonika* **63**, 73–79 (2018).

100. Yeom, H. *et al.* Magnetron sputter deposition of zirconium-silicide coating for mitigating high temperature oxidation of zirconium-alloy. *Surf. Coatings Technol.* **316**, 30–38 (2017).

101. Cheol Lee, G. *et al.* Zirconium-silicide coating on zircaloy-4 substrate for accident tolerance: Effects on oxidation resistance and boiling. *Ann. Nucl. Energy* **126**, 350–358 (2019).

102. Kim, J., Kim, H. G. & Ryu, H. J. High Temperature Oxidation Behavior of ZrSi2 and Its Coating on the Surface of Zircaloy-4 Tube by 3D Laser Coating Method. in *Transactions of the Korean Nuclear Society Spring Meeting* 1–4 (2018).

103. Son, G. M., Kim, K. M. & Bang, I. C. Chromia coating with nanofluid deposition and sputtering for accident tolerance, CHF enhancement. *Int. J. Heat Mass Transf.* **118**, 890–899 (2018).

104. Bao, W. *et al.* Coating SiC on Zircaloy-4 by magnetron sputtering at room temperature. *J. Alloys Compd.* **730**, 81–87 (2018).

105. Lee, K., Kim, D. & Yoon, Y. S. SiC/Si thin film deposited on zircaloy to improved accident tolerant fuel cladding. *Thin Solid Films* **660**, 221–230 (2018).

106. Ren, D. *et al.* Synthesis of Zr2Al3C4 coatings on zirconium-alloy substrates with Al C/Si interlayers as diffusion barriers. *Vacuum* **160**, 128–132 (2018).

107. Tang, C. *et al.* Evaluation of magnetron sputtered protective Zr-Al-C coatings for accident tolerant Zircaloy claddings. in *2017 Water Reactor Fuel Performance Meeting* 1–9 (2017).

108. Khatkhatay, F. *et al.* Superior corrosion resistance properties of TiN-based coatings on Zircaloy tubes in supercritical water. *J. Nucl. Mater.* **451**, 346–351 (2014).

109. Kuprin, A. S. *et al.* Vacuum-arc chromium-based coatings for protection of zirconium alloys from the high-temperature oxidation in air. *J. Nucl. Mater.* **465**, 400–406 (2015).

110. Sagás, J. C. *et al.* Energetic particle irradiation study of TiN coatings: are these films

appropriate for accident tolerant fuels? *J. Nucl. Mater.* **512**, 239–245 (2018).

111. Ren, Y. *et al.* Effect of roughness of substrate and sputtering power on the properties of TiN coatings deposited by magnetron sputtering for ATF. *J. Nucl. Mater.* **509**, 542–549 (2018).

112. Wu, Y. *et al.* Study of the oxidation behavior of CrN coating on Zr alloy in air. *J. Nucl. Mater.* **515**, 354–369 (2019).

113. Liu, Y. *et al.* Evaluation of the interfacial shear strength and residual stress of TiAlN coating on ZIRLO™ fuel cladding using a modified shear-lag model approach. *J. Nucl. Mater.* **466**, 718–727 (2015).

114. Brova, M. J. *et al.* Undoped and ytterbium-doped titanium aluminum nitride coatings for improved oxidation behavior of nuclear fuel cladding. *Surf. Coatings Technol.* **331**, 163–171 (2017).

115. Daub, K., Nieuwenhove, R. Van & Nordin, H. Investigation of the impact of coatings on corrosion and hydrogen uptake of Zircaloy-4. *J. Nucl. Mater.* **467**, 260–270 (2015).

116. Tang, C. *et al.* H2 permeation behavior of Cr2AlC and Ti2AlC MAX phase coated Zircaloy-4 by neutron radiography. *Acta Polytech.* **58**, 69–76 (2018).

117. Maier, B. R. *et al.* Cold spray deposition of Ti2AlC coatings for improved nuclear fuel cladding. *J. Nucl. Mater.* **466**, 712–717 (2015).

118. Yeom, H. *et al.* Laser surface annealing and characterization of Ti2AlC plasma vapor deposition coating on zirconium-alloy substrate. *Thin Solid Films* **615**, 202–209 (2016).

119. Wang, J. *et al.* Microstructure evolution of V2AlC coating on Zr substrate under He irradiation and their mechanical behavior. *Scr. Mater.* **137**, 13–17 (2017).

120. Tang, C. *et al.* Deposition, characterization and high-temperature steam oxidation behavior of single-phase Ti2AlC-coated Zircaloy-4. *Corros. Sci.* **135**, 87–98 (2018).

121. Zhang, J., Tian, Z., Zhang, H., Zhang, L. & Wang, J. On the chemical compatibility between Zr-4 substrate and well-bonded Cr2AlC coating. *J. Mater. Sci. Technol.* **35**, 1–5 (2019).

122. Tallman, D. J., Anasori, B. & Barsoum, M. W. A Critical Review of the Oxidation of Ti2AlC, Ti3AlC2 and Cr2AlC in Air. *Mater. Res. Lett.* **1**, 115–125 (2013).

123. Tang, C. *et al.* Improvement of the High-Temperature Oxidation Resistance of Zr Alloy Cladding by Surface Modification with Aluminum-Containing Ternary Carbide Coatings. in *International Congress on Advances in Nuclear Power Plants* 694–700 (2018).

124. Ward, J. *et al.* Corrosion performance of Ti3SiC2, Ti3AlC2, Ti2AlC and Cr2AlC MAX phases in simulated primary water conditions. *Corros. Sci.* **139**, 444–453 (2018).

125. Ivanova, S. V., Glagovsky, E. M., Nikonorov, K. Y., Belugin, I. I. & Khazov, I. A. Methods to increase corrosion stability and wear resistance of LWR active core zirconium components during operation and in conditions of loss-of-coolant accident. in *Proceedings of TopFuel 2013* 334–350 (2013).

126. Zhang, W. *et al.* Preparation, structure, and properties of high-entropy alloy multilayer coatings for nuclear fuel cladding: A case study of AlCrMoNbZr/(AlCrMoNbZr)N. *J. Nucl. Mater.* **512**, 15–24 (2018).

127. Zhang, W. *et al.* Interface stability, mechanical and corrosion properties of AlCrMoNbZr/(AlCrMoNbZr)N high-entropy alloy multilayer coatings under helium ion

irradiation. *Appl. Surf. Sci.* **485**, 108–118 (2019).

128. Lee, Y., Lee, J. I. & NO, H. C. Mechanical analysis of surface-coated zircaloy cladding. *Nucl. Eng. Technol.* **49**, 1031–1043 (2017).

129. Lee, Y. H. *et al.* Enhanced wear resistance of CrAl-coated cladding for accident-tolerant fuel. *J. Nucl. Mater.* **523**, 223–230 (2019).

130. Capps, N., Mai, A., Kennard, M. & Liu, W. PCI analysis of Zircaloy coated clad under LWR steady state and reactor startup operations using BISON fuel performance code. *Nucl. Eng. Des.* **332**, 383–391 (2018).

131. Zinkle, S. J. & Busby, J. T. Structural materials for fission & fusion energy. *Mater. Today* **12**, 12–19 (2009).

132. Kratochvílová, I. *et al.* Nanosized polycrystalline diamond cladding for surface protection of zirconium nuclear fuel tubes. *J. Mater. Process. Technol.* **214**, 2600–2605 (2014).

133. Bugnet, M., Mauchamp, V., Oliviero, E., Jaouen, M. & Cabioc'h, T. Chemically sensitive amorphization process in the nanolaminated Cr2AC (A = Al or Ge) system from TEM in situ irradiation. *J. Nucl. Mater.* **441**, 133–137 (2013).

134. Gigax, J. G. *et al.* Radiation response of Ti2AlC MAX phase coated Zircaloy-4 for accident tolerant fuel cladding. *J. Nucl. Mater.* **523**, 26–32 (2019).

135. Field, K. G., Briggs, S. A., Sridharan, K., Howard, R. H. & Yamamoto, Y. Mechanical properties of neutron-irradiated model and commercial FeCrAl alloys. *J. Nucl. Mater.* **489**, 118–128 (2017).

136. Sridharan, K. *et al.* Irradiation-enhanced α ′ precipitation in model FeCrAl alloys. *Scr. Mater.* **116**, 112–116 (2016).

137. Xiao, J., Yang, T., Wang, C., Xue, J. & Wang, Y. Investigations on Radiation Tolerance of Mn+1AXn Phases: Study of Ti3SiC2, Ti3AlC2,Cr2AlC, Cr2GeC, Ti2AlC, and Ti2AlN. *J. Am. Ceram. Soc.* **98**, 1323–1331 (2015).

138. Tallman, D. J. *et al.* Effect of neutron irradiation on select MAX phases. *Acta Mater.* **85**, 132–143 (2015).

139. Wang, C. *et al.* Role of the X and n factors in ion-irradiation induced phase transformations of M n+1 AX n phases. *Acta Mater.* **144**, 432–446 (2018).

140. Ang, C. *et al.* Anisotropic swelling and microcracking of neutron irradiated Ti3AlC2-Ti5Al2C3 materials. *Scr. Mater.* **114**, 74–78 (2016).

141. Shen, H. H. *et al.* He+ irradiation induced cracking and exfoliating on the surface of Ti3AlC2. *J. Nucl. Mater.* **485**, 262–272 (2017).

142. Shah, H. *et al.* Westinghouse-Exelon EnCore ® Fuel Lead Test Rod (LTR) Program including Coated cladding Development and Advanced Pellets. in *TOPFUEL* 1–9 (2018).

143. Nieuwenhove, R. Van, Andersson, V., Balak, J. & Oberländer, B. In-pile testing of CrN, TiAlN and AlCrN Coatings on Zircaloy cladding in the Halden Reactor. in *18th International Symposium on Zirconium in the Nuclear Industry* 965–982 (2018). doi:10.1520/STP159720160011

144. Lee, K.-G., In, W.-K. & Kim, H.-G. Quenching experiment on Cr-alloy-coated cladding for accident-tolerant fuel in water pool under low and high subcooling conditions. *Nucl. Eng. Des.* **347**, 10–19 (2019).

145. Seshadri, A., Phillips, B. & Shirvan, K. Towards understanding the effects of

irradiation on quenching heat transfer. *Int. J. Heat Mass Transf.* **127**, 1087–1095 (2018).

146. Meschter, P. J., Opila, E. J. & Jacobson, N. S. Water Vapor–Mediated Volatilization of High-Temperature Materials. *Annu. Rev. Mater. Res.* **43**, 559–588 (2013).

147. Young, D. J. *High Temperature Oxidation and Corrosion of Metals*. *Corrosion Series* **1**, (Elsevier, 2008).

148. Carr, J., Vasudevamurthy, G., Snead, L., Hinderliter, B. & Massey, C. Investigations of Aluminum-Doped Self-Healing Zircaloy Surfaces in Context of Accident-Tolerant Fuel Cladding Research. *J. Mater. Eng. Perform.* **25**, 2347–2355 (2016).

149. Lukas, H., Fries, S. G. & Sundman, B. *Computational thermodynamics: the Calphad method*. (Cambridge university press, 2007).

150. Kim, H.-G., Kim, I.-H., Park, J.-Y. & Koo, Y.-H. Application of Coating Technology on Zirconium-Based Alloy to Decrease High-Temperature Oxidation. *Zircon. Nucl. Ind. 17th Vol.* 346–369 (2014). doi:10.1520/stp154320120161

151. Dong, Y. *et al.* Improved oxidation resistance of zirconium at high-temperature steam by magnetron sputtered Cr-Al-Si ternary coatings. *Surf. Coatings Technol.* **350**, 841–847 (2018).

152. Terrani, K. A., Parish, C. M., Shin, D. & Pint, B. A. Protection of zirconium by alumina- and chromia-forming iron alloys under high-temperature steam exposure. *J. Nucl. Mater.* **438**, 64–71 (2013).

153. Gigax, J. G. *et al.* Interface reactions and mechanical properties of FeCrAl-coated Zircaloy-4. *J. Nucl. Mater.* **519**, 57–63 (2019).

154. Han, X., Wang, Y., Peng, S. & Zhang, H. Oxidation behavior of FeCrAl coated Zry-4 under high temperature steam environment. *Corros. Sci.* **149**, 45–53 (2019).

155. Westwood, M. E., Webster, J. D., Day, R. J., Hayes, F. H. & Taylor, R. Oxidation protection for carbon fibre composites. *J. Mater. Sci.* **31**, 1389–1397 (1996).

156. Mayrhofer, P. H., Rachbauer, R., Holec, D., Rovere, F. & Schneider, J. M. *Protective Transition Metal Nitride Coatings*. *Comprehensive Materials Processing* **4**, (Elsevier, 2014).

157. Qi, Z. B., Wu, Z. T. & Wang, Z. C. Improved hardness and oxidation resistance for CrAlN hard coatingswith Y addition by magnetron co-sputtering. *Surf. Coatings Technol.* **259**, 146–151 (2014).

158. Skarohlid, J. & Skoda, R. High temperature behaviour of CrAlSiN MAX phase coatings on zirconium alloy. in *Water Reactor Fuel Performance Meeting* 1–5 (2017).

159. Ma, X. F. *et al.* Evaluation of corrosion and oxidation behaviors of TiAlCrN coatings for nuclear fuel cladding. *Surf. Coatings Technol.* **358**, 521–530 (2019).

160. Li, S., Song, G., Kwakernaak, K., van der Zwaag, S. & Sloof, W. G. Multiple crack healing of a Ti2AlC ceramic. *J. Eur. Ceram. Soc.* **32**, 1813–1820 (2012).

161. OuYang, X. *et al.* Experimental investigation and thermodynamic calculation of the B-Fe-W ternary system. *Calphad Comput. Coupling Phase Diagrams Thermochem.* **63**, 212–219 (2018).

162. Hajas, D. E. *et al.* Oxidation of Cr2AlC coatings in the temperature range of 1230 to 1410°C. *Surf. Coatings Technol.* **206**, 591–598 (2011).